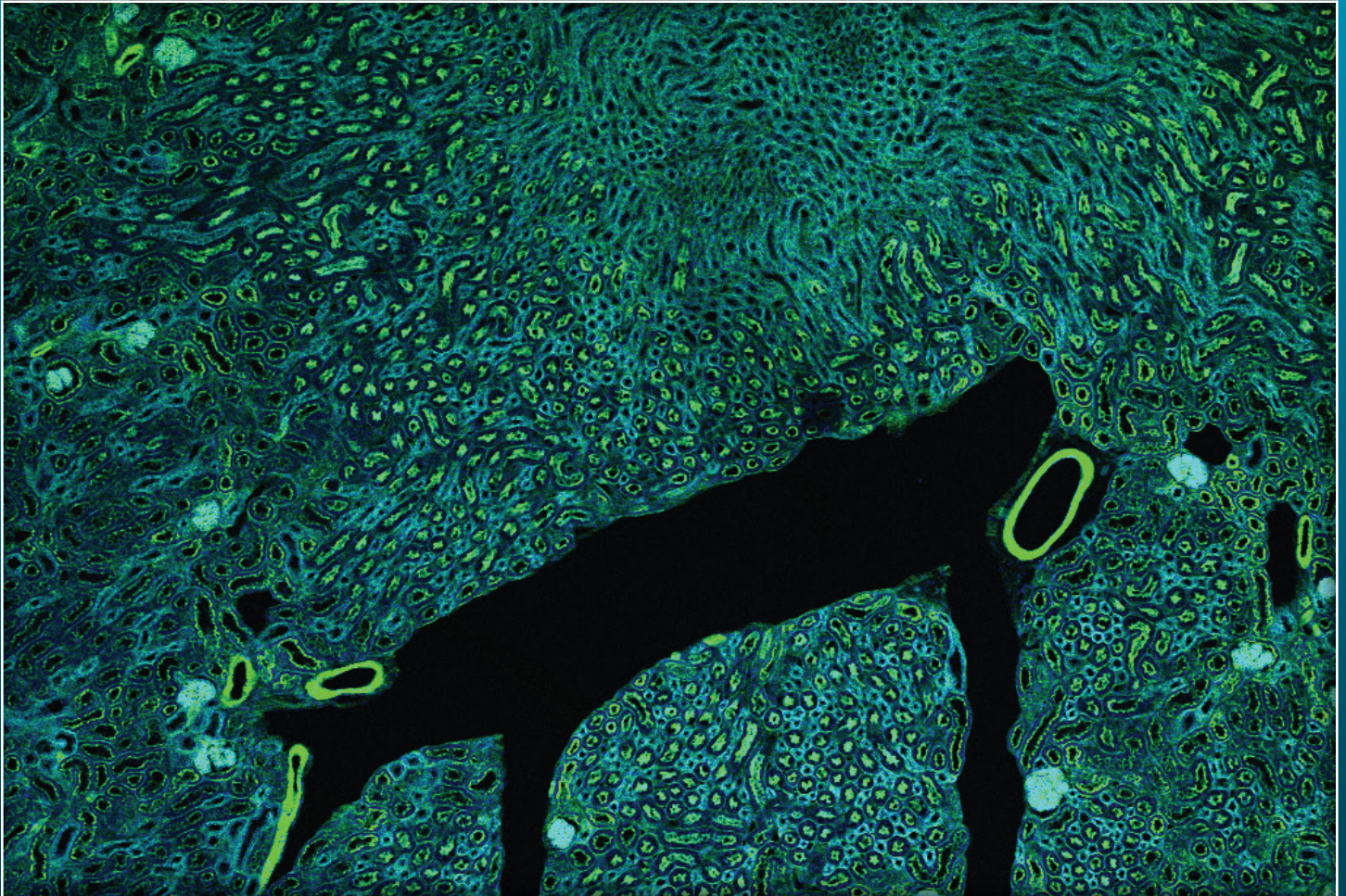


Texas Journal of Microscopy



Volume 56

Number 1, 2025

ISSN 1554-0820

Visit our website at <https://texas.microscopy.org/>

DiATOME

Diamond Knives

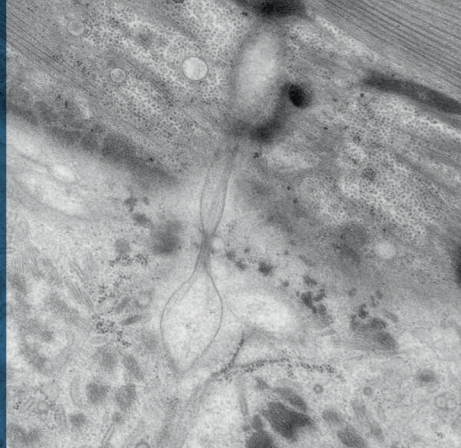
the incomparable
Diamond Knife for all
fields of research...

Please visit our website for our complete range:
www.diatomeknives.com



ultra 35°

Perfect for sectioning relatively soft materials research specimens including metals and polymers, as well as mixed specimens such as polymers filled with nanoparticles, brittle materials such as catalysts, crystals, semiconductors, etc. The ultra 35° knife has demonstrated its usefulness as a standard knife for a majority of applications in both biological and materials research.



Ultrastructure of the roundworm *Caenorhabditis elegans*.
Thomas Müller-Reichert, EM Technology Development, MPI Dresden, and Kent McDonald, Electron Microscopy Laboratory, University of California, Berkeley.

ultra-semi 35°

Similar to our ultra 35° 3.0 mm with a greater thickness range (50-200nm). Ideal for alternating sectioning from ultrathin to semithin.

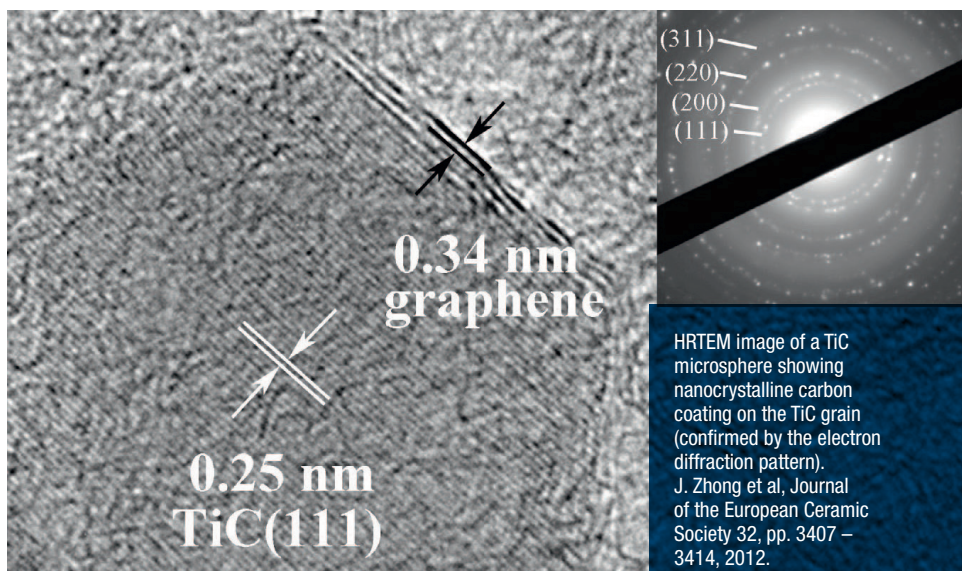
ultra 35° (dry)

The ultra 35° knife (in the triangular holder) with a thickness range of 30-200nm is used for dry sectioning of epoxy or acrylic resin embedded biological samples, which need to be investigated by element analysis (Ref. Edelmann) and SIMS (Ref. Guerquin-Kern). The gliding of the sections on the dry knife surface is facilitated with the use of our Static Line II Ionizer.



ultra 45°

Acknowledged as the appropriate knife angle for routine sectioning of both biological and materials research specimens, it represents a balanced compromise between section quality and durability.



HRTEM image of a TiC microsphere showing nanocrystalline carbon coating on the TiC grain (confirmed by the electron diffraction pattern).
J. Zhong et al, Journal of the European Ceramic Society 32, pp. 3407 – 3414, 2012.

DiATOME U.S.

www.diatomeknives.com

314 West Broad Street, Suite 203
Quakertown, PA 18951
Tel: (215) 412-8390 or 215-646-1478
email: info@diatomeknives.com

TSM OFFICERS 2024-2025

President:

JOSEFINA ARELLANO
MSE Core Characterization Facility
The University of Texas at Dallas | Richardson, TX 75080
(972) 883-5759
Josefina.Arellano@utdallas.edu

President-elect:
VACANT

Past President:

AMY JO HAMMETT
Department of Biological Sciences
The University of Texas at Dallas | Richardson, TX 75080
AmyJo.Hammett@UTDallas.edu

Secretary:

JOYCE ANDERSON
Shared Research Operations
Texas State University | San Marcos, TX 78666
Email: jha39@txstate.edu

Secretary-elect:
VACANT

Treasurer:

BERND ZECHMANN
Center for Microscopy and Imaging
Baylor University | Waco, TX 76798-7046
(254) 710-2322
Bernd_Zechmann@baylor.edu

Treasurer-elect:
VACANT

Program Chairperson:

MUNENORI ISHIBASHI
College of Optometry | University of Houston
Houston, Texas 77004
Email: mishibas@Central.UH.EDU

Program Chairperson-elect:
VACANT

APPOINTED OFFICERS

Corporate Member Representative:

JOHN HARITOS
Gatan/EDAX
Email: john.haritos@ametec.com

Marketing and Outreach Officer:
VACANT

Student Representative:

TAYLOR JEFFERIS
Department of Environmental Sciences
Baylor University | Waco, TX 76798-7046
Email: taylor_jefferis1@baylor.edu

Journal Editors:

JOYCE ANDERSON, JOSEFINA ARELLANO,
JOHN HARITOS, MUNENORI ISHIBASHI,
BERND ZECHMANN

Webmaster:

BERND ZECHMANN
Center for Microscopy and Imaging
Baylor University | Waco, TX 76798-7046
(254) 710-2322
Bernd_Zechmann@baylor.edu

Contents

TEXAS JOURNAL OF MICROSCOPY
VOLUME 56, NUMBER 1, 2025
ISSN 1554-0820



Editors

Joyce Anderson, Josefina Arellano,
John Haritos, Munenori Ishibashi,
Bernd Zechmann

Official Journal of the Texas Society for Microscopy
“TSM - Embracing all forms of Microscopy”

<https://texas.microscopy.org/>

President's Message	4
Keynote Speakers for the 59th TSM Meeting.....	5-6
Spring 2025 Life Sciences Abstracts.....	7-17
Spring 2025 Materials Science Abstracts.....	18-28
Spring 2025 Education Abstracts.....	29
Corporate Members.....	31-34
Advertiser's Index:	
DiAtome	2
Electron Microscopy Science	30
Nikon	35
Rigaku	36

ON THE COVER

Fairbairn-Stained Mouse Kidney: Image of a mouse kidney taken with an Olympus FV3000 Laser Scanning Confocal Microscope at 5x magnification. The micrograph was obtained by Nicki Fairbairn, Scientific Instrument Technician at Shared Research Operations, Texas State University, San Marcos.

President's Message

Dear Members of the Texas Society for Microscopy,

This year we are celebrating the 59th edition of our annual meeting and I feel so proud and grateful for the amazing community we have built together. The Texas Society for Microscopy continues to thrive, thanks to the dedication and passion of our members who are leading the way in advancing microscopy and its applications.

Last year, we saw some incredible achievements and breakthroughs in our field. Our 58th TSM meeting was a huge success, with groundbreaking research presentations, insightful discussions, and great networking opportunities. The enthusiasm and engagement of our members were truly inspiring. Thank you again to Joyce Anderson and the amazing group of volunteers from the Shared Research Operations Facility, at Texas State University, in San Marcos.

In 2025, our program chairperson Munenori (Nori) Ishibashi has prepared an exciting program. We are delighted to support and display the hard work of our members and we look forward to this year's platform and poster presentations. A special thank you to our invited speakers, Stefanie N. Milam from NASA Goddard Space Flight Center, and Irina I. Serysheva from The University of Texas Health Science Center at Houston, for their support. I want to extend a big thank you to our board members: Joyce Anderson, John Haritos, Munenori Ishibashi, Taylor Jefferis, and Bernd Zechmann, and to our volunteers and sponsors for their continuous support. Your contributions are the backbone of our society, making all our achievements possible. I also want to acknowledge the hard work of our editorial team, who work diligently

on the content for the Texas Journal of Microscopy.

Looking ahead, we have big plans. We are excited to announce the launch of our new website. Stay tuned for more details and explore the new features! We aim to continue our educational initiatives and collaborate more with other scientific communities. We encourage our members to apply to the Small Grant program and submit your micrographs to the image competition. TSM remains active among the group of Local Affiliated Societies of the Microscopy Society of America. We're committed to supporting our members' professional growth and providing platforms for them to showcase their work.

As we move forward, I encourage each of you to stay engaged, share your ideas, and actively participate in our events and initiatives. Together, we can continue to advance the microscopy community and make significant contributions to science and society. We're always looking for passionate individuals to join our leadership team. If you're enthusiastic about making a difference and shaping the future of microscopy, I invite you to volunteer and become a member of our board. Your unique perspectives and skills are invaluable, and your involvement will help us achieve our goals. Please reach out to us to learn more about how you can contribute and take on a leadership role within TSM.

Thank you for your continued commitment to TSM. I look forward to a productive and engaging meeting.

Warm regards,

Josefina Arellano

President, The Texas Society for Microscopy.



NEW EYES FOCUSED ON THE UNIVERSE: HOW THE JAMES WEBB SPACE TELESCOPE IS REVEALING OUR MOLECULAR ORIGINS

Stefanie N. Milam

Astrochemistry Laboratory, NASA Goddard Space Flight Center, Greenbelt, MD, United States.



In late 2021, the James Webb Space Telescope (JWST) was launched to the Sun-Earth Lagrange point 2 (L2), approximately 1.5 million kilometers (~1 million miles) from Earth. Over 25 years in the making, JWST has been one of the most challenging programs, but also extremely rewarding, in its first 3 year of science operations for NASA, ESA, and CSA as well as for all astronomers and the public. This telescope has unprecedented sensitivity and angular resolution and is the premier space-based facility for near- and mid-infrared (0.6-28.5 μm) astronomy. A true engineering challenge was deploying the 6.5-meter primary mirror and 21-meter-long sunshield in the vacuum of space. The telescope is equipped with four state-of-the-art instruments which include imaging, spectroscopy, and coronagraphy modes. These instruments are returning amazing spectra and images of the most distant galaxies known to date and even objects much closer to home in our Solar System. JWST is revealing the composition and dynamic processes of these objects not readily accessible with other observatories or even planetary missions.

The spectral capability of JWST enables detailed studies on composition of objects beyond Earth's atmosphere. Key volatile species, ices, dust and grains, etc. can be studied with exquisite sensitivity to gain insight into the distribution and evolution of molecular and macromolecular materials throughout cosmic time. JWST has already made multiple new discoveries and

will continue to do so as new questions emerge from this new data.

The nominal launch and efficient operations in place ensure a JWST science mission lifetime of up to 20 years, enabling new discoveries and exploration for future generations. This presentation will highlight some of the engineering challenges for the telescope and some new discoveries from the microscopic perspective JWST enables throughout the cosmos.

Dr. Milam works in the Astrochemistry Laboratory at the NASA Goddard Space Flight Center. She is an expert in rotational spectroscopy, observations, and laboratory modeling of astrochemistry and molecular astrophysics of the interstellar medium, evolved stars, star formation regions, and comets. Her observational focus is on the compositional studies of primitive bodies, namely comets and interstellar objects, and uses ground- and space-based facilities to understand their connection to the formation and evolution of planetary systems. She also has a laboratory dedicated to simulate interstellar/cometary/planetary ices. Dr. Milam has been working on the James Webb Space Telescope (JWST) as Deputy Project Scientist for Planetary Science since 2014. Under this role she has helped enable observations within our own solar system from Near-Earth Asteroids to the farthest reaches of the Kuiper belt and even the brightest objects in the infrared sky (e.g. Mars). She has also led the study team for solar system science for the Roman Space Telescope. In 2021, she was honored with asteroid 40706 (1999 RO240) was renamed to 40706 Milam. She received the NASA Exceptional Scientific Achievement Medal in 2022 for her work on enabling Solar System Science with JWST.

DECODING THE IP₃R CHANNEL FUNCTION THROUGH CRYO-EM STUDIES

Irina I. Serysheva, PhD

Professor

Department of Biochemistry and Molecular Biology

Director of Structural Biology Imaging Center

McGovern Medical School UTHealth at Houston, TX



The structural basis of Ca²⁺ transport represents one of the most important and challenging frontiers in structural biology. Ion channels, a class of integral membrane proteins, mediate the passive transport of ions across biological membranes, driven by the electrochemical gradients. The structural

determination of ion channels remains a formidable challenge due to their intrinsic dynamic nature and functional reliance on complex lipid membrane environments. Over the past decade, cryo-EM has emerged as a transformative technology, enabling unprecedented insights into the structures of membrane proteins, including ion channels. In this talk, I will focus on cryo-EM studies of inositol 1,4,5-trisphosphate receptors (IP3Rs), which serve as key intracellular Ca²⁺ channels critical for a wide range of cellular signaling pathways. I will discuss the unique challenges associated with determining the structures of IP3R channels using single-particle cryo-EM, highlighting the complexities introduced by their dynamic conformations and interactions within lipid membranes. I will showcase the significant progress made in achieving atomic-resolution structures of IP3Rs in various functional states and lipid environments, shedding light on the

molecular mechanisms governing their structure and activity. Additionally, I will delve into the most recent advancements in cryo-EM technology, including the integration of machine-learning approaches. These cutting-edge methods have expanded our ability to explore the conformational landscape of proteins, allowing for a deeper insight into their structural dynamics as captured in cryo-EM images.

Dr. Irina Serysheva is the Jesse H. Jones Chair in Molecular Biology and a Professor in the Department of Molecular Biology and Biochemistry at UTHealth McGovern Medical School at Houston. She also serves as the Director of the Cryo-EM Core Facility at UTHealth. Dr. Serysheva's research spans a wide range of critical areas, including molecular transport across biological membranes, the structure-function relationships of membrane proteins, cellular signaling mechanisms, cryo-EM of biological macromolecules. Her work also focuses on the molecular mechanisms underlying neurodegeneration and neuronal health. Dr. Serysheva is an internationally recognized leader in ion channel research. She achieved a groundbreaking milestone as the first scientist to determine the three-dimensional structure of the inositol 1,4,5-trisphosphate receptor, a pivotal ion channel that regulates calcium transport in nearly all human tissues. Dr. Serysheva has an extensive publication record in leading scientific journals, including *Nature*, *Nature Communications*, *Science*, *PNAS*, *Structure*, and *Cell Research*, among others.

SINGLE CELL SPATIAL PROTEOMICS ANALYSIS AND COMPUTATIONAL EVALUATION PIPELINE.

Behnaz Bozorgui¹, Guillaume Thibault², Zeynep Dereli¹, John N Weinstein¹, Anil Korkut¹.

¹Department of Bioinformatics and Computational Biology, UT MD Anderson Cancer Center, ²Cancer Early Detection Advanced Research Center, Oregon Health Science Center University.

Resolving tissue and proteomic heterogeneity is critical to decoding the structure and function of tumor-immune microenvironment (TIME). Such understanding requires profiling of tumor and immune cell proteomic features with spatial resolution at the single-cell level. Although such spatially resolved methods and data sets are becoming increasingly available, analytical and computational methods that can extract the highly complex features and interactions within TIME are lacking. Moreover, due to drug-induced structural changes in tissues or structural difference in normal and tumor tissues, defining features that are comparable across multiple tissue types remain challenging.

Here we introduce spatial proteomics analysis and computational (SPACE) pipeline composed of many analysis modules for processing and mining highly multiplexed imaging-based data types to explore TIME composition, organization, and heterogeneity. The pipeline generates and interprets biomarker expression and positional information from multiplexed images using algorithms for image indexing, image registration, quality control, segmentation, identification and removal of non-specific signals, data normalization, automatic identification of missing data and lost tissue and adjustment for left-over signals. The accurate intensity measurements at single cell level are then used to calculate the proposed spatial features that represent cellular interactions in TIME. A hierarchical decision tree of cell markers is used to annotate types and identities for individual cells. A novel expression-weighted proximity score is defined for entities such as single cells and proteins to inform on spatial enrichment, cellular neighborhoods, and ligand-receptor interactions in proximity. Normalized by the structural components of tissue our spatial enrichment score makes spatial enrichment comparable across tissues with different intrinsic structures such as tumor and normal tissue.

A novel expression-weighted proximity score, called SPACE enrichment scores, is defined for single cell as

well as proteins to inform on spatial enrichment, cellular neighborhoods, and ligand-receptor interactions in proximity, and identify new tissue domains and cellular subtypes. Normalized by the structural components of tissue, SPACE enrichment scores make spatial enrichment comparable across tissues with different intrinsic structures and provides a universal metric for molecular enrichment. SPACE enrichment scores thus provide an ideal tool for differential analysis of spatial transcriptomic profiles of structurally-distinct micro environments such as in tumor and normal tissues, tissues that undergo drug-induced structural changes, or different cancer types.

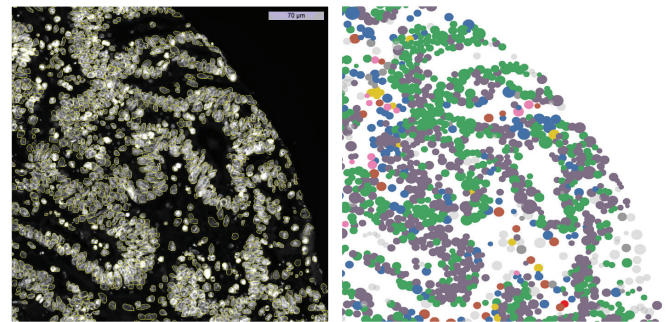


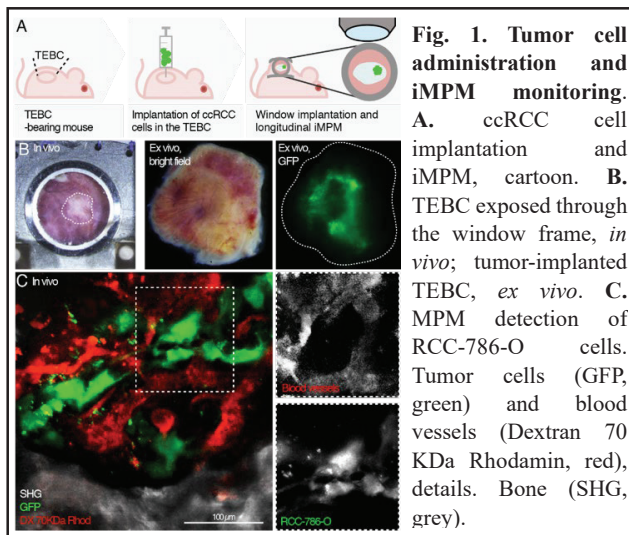
Fig 1. Left: DAPI-stained Nuclei of small bowel tissue imaged using cyclic immunofluorescence experiment and segmented using MASK R-CNN model incorporated in SPACE. Scale bar is 70 μ m. **Right:** Spatial map of cell phenotypes using SPACE-extracted protein features and user-input hierarchical classification tree.

INTEGRATED MODELING OF RENAL CANCER BONE METASTASIS TO ILLUMINATE AND OVERCOME THERAPY FAILURE.

Sergio Barrios¹, Stefan Maksimovic¹, Luca Marsilio², Matthew Campbell¹, Stefano Casarin², Eleonora Dondossola¹.

¹Department of Genitourinary Medical Oncology, The University of Texas MD Anderson Cancer Center, Houston, TX 77030, USA. ²Department of Surgery, Houston Methodist, Houston, TX, 77030, USA.

Bone metastatic clear cell renal cell carcinoma (BM ccRCC) is a persistent clinical challenge and a source of significant morbidity and lethality for up to 40% of metastatic patients. Despite the recent approval of life-prolonging agents (antiangiogenic agents, immunotherapy) patients with BM ccRCC will eventually progress, due to emerging resistance. Bidirectional communication between cancer cells and bone stroma has emerged as a driver of disease



progression and relapse. However, a major challenge in addressing the black box of therapy response in bone is a lack of efficient, informative systems that allow us to dissect heterotypic stromal-epithelial interplay, which is further complicated by the anatomical inaccessibility of bone. For these reasons, the evolution of the metastatic resistance niche and its implications in therapy response remain elusive.

In order to improve clinical results, it is critical moving forward to establish biologically informed pre-clinical models to provide a mechanistic understanding of tumor progression in bone and treatment outcomes. To this purpose, we have established clinically relevant models of ccRCC bone metastasis that span *in vivo* and *ex vivo* multiphoton microscopy (iMPM and eMPM), tissue engineered bone window systems, and computational oncology.

iMPM displays both sensitivity and time-resolution to identify dynamic interactions between ccRCC cells and bone 3D adaptive niches, which support therapy response and resistance [Fig. 1]. However, iMPM in bone is limited due to its cortical thickness, increased light scattering, and complex topology. As a novel alternative, we created a tissue-engineered bone construct (TEBC) that, after direct implantation of cancer cells, is combined with an adjacent skin window, allowing for non-destructive intravital examination of tumor growth. To flank these *in vivo* dynamic analyses, we established a pipeline for *ex vivo* extraction of topological information related to the molecular and cellular niches involved in tumor progression and response to antiangiogenic treatment. This method allows reconstruction of whole lesions, including zones more distant from the bone interface, paired with an extensive panel of molecular markers. To further investigate the effects of a broad multi-parameter space on tumor regression or persistence upon antiangiogenic treatment, *in silico*, we developed an *in vivo*-inspired agent-based model (ABM) of ccRCC

in bone. A computational approach combined to ad hoc biological experimentation can refine the experimental design, test clinically relevant hypotheses (including impact of treatments on disease progression) and predict scenarios that guide biological testing towards more successful outcomes.

As a result, by integrating these approaches, we are currently investigating the progression of the bone metastatic niche and its response to the therapy, with the final aim to overcome therapy failure.

ACTIVATED FIBROBLASTS IN CELL-SEEDED SCAFFOLDS TO MITIGATE THE FOREIGN BODY RESPONSE.

Asieh Etemad¹, Vasiliki Kolliopoulos^{1,2}, Antonios G Mikos², Eleonora Dondossola¹. ¹Department of Genitourinary Medical Oncology and David H. Koch Center for Applied Research of Genitourinary Cancers, The University of Texas MD Anderson Cancer Center, Houston, TX 77030, USA. ²department of Bioengineering, Rice University, Houston, TX 77030, USA.

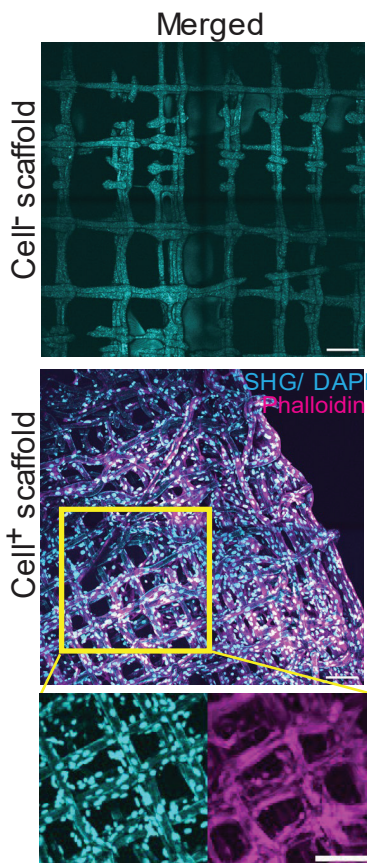


Fig 1. Representative image of scaffold plus (+) and minus (-) cells. SHG/DAPI in Cyan; Phalloidin in magenta, Scale bar: 200 μ m, Inset 100 μ m,

The foreign body response (FBR) is the body's immune reaction to foreign materials, involving inflammation, macrophage activation, and fibrosis. It aims to isolate or eliminate the foreign object but can lead to complications like scarring or implant failure^{1,2}. In the progression of FBRs, macrophages regulate inflammation and healing by polarizing pre-inflammatory or anti-inflammatory responses and recruit fibroblasts by secreting cytokines¹. In turn, fibroblasts activate and deposit collagen, forming scar tissue (fibrosis) that shield the foreign material from the host.

Different concepts have been explored to attenuate the FBR and fibrosis. One approach to mitigate FBR is to use biomimetic materials that mimic the structures, properties, or functions of native

tissues 3. As an alternative, functionalizing implantable biomaterials with cells represents an approach to increase biocompatibility⁴.

Here we applied intravital multiphoton microscopy (iMPM) to compare the FBR elicited by polycaprolactone (PCL) scaffolds that were either functionalized or not functionalized with mouse-derived cells [Fig.1]. To monitor the dynamics of both immune cells and fibroblasts, we implanted the scaffolds in a skin window (dorsal skinfold chamber, DSFC) on the back of α SMA-RFP/GFP dual reporter mice¹. Preliminary experiments in mice implanted with scaffolds, either with or without cells, showed reduced recruitment of immune cells and α SMA-positive fibroblasts in functionalized scaffolds. These results suggest that the FBR dynamics might be downregulated by incorporating a biological live component to biomaterials.

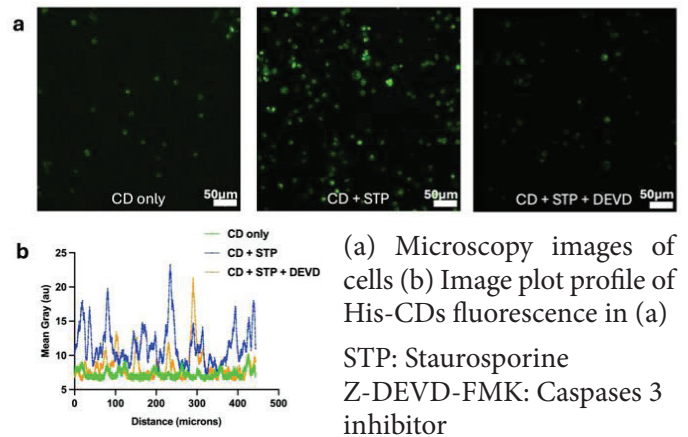
- 1 Parlani, M., Bedell, M. L., Mikos, A. G., Friedl, P. & Dondossola, E. Dissecting the recruitment and self-organization of α SMA-positive fibroblasts in the foreign body response - PubMed. *Science advances* 8 (2022). <https://doi.org/10.1126/sciadv.add0014>
- 2 Dondossola, E., Friedl, P., Dondossola, E. & Friedl, P. Host responses to implants revealed by intravital microscopy. *Nature Reviews Materials* 2021 7:1 7 (2021). <https://doi.org/10.1038/s41578-021-00369-x>
- 3 Zhou, X., Wang, Y., Ji, J. & Zhang, P. Materials Strategies to Overcome the Foreign Body Response. *Advanced Healthcare Materials* 13 (2024). <https://doi.org/10.1002/adhm.202304478>
- 4 Alhag, M. et al. Evaluation of early healing events around mesenchymal stem cell-seeded collagen-glycosaminoglycan scaffold. An experimental study in Wistar rats. *Oral and Maxillofacial Surgery* 2010 15:1 15 (2010). <https://doi.org/10.1007/s10006-010-0241-x>

HISTIDINE-DERIVED CARBON DOTS AS FLUORESCENT PROBES FOR DETECTING STAUROSPORINE-INDUCED APOPTOSIS

Hammed Faleke and Dimitri. Pappas. Department of Chemistry and Biochemistry, Texas Tech University Lubbock, TX 79409-1061

Histidine-derived carbon dots (His-CDs) were synthesized to detect staurosporine-induced apoptosis in T lymphoma (Jurkat) cells. The His-CDs were characterized for their physical and chemical properties, including size, morphology, fluorescence, and surface functionality. Transmission electron microscopy (TEM) revealed a spherical morphology with an average size of

11.4 \pm 3.4 nm. Fluorescence analysis showed maximum excitation at 338 nm and emission at 415 nm, attributed to the carbon dots' quantum confinement effect and surface defects. Fourier Transform Infrared spectroscopy (FTIR) indicates the presence of hydroxyl, amine, aromatic rings, and alkyl functional groups. Scanning electron microscopy and energy dispersive X-ray spectroscopy (SEM-EDS) further reveal that His-CDs consist of 52.0% carbon, 24.8% nitrogen, and 23.3% oxygen. His-CDs were evaluated for cytotoxicity and apoptosis detection in Jurkat cells. Fluorescence microscopy and flow cytometry analysis demonstrated concentration-dependent fluorescence, suggesting effective cellular uptake of His-CDs. The apoptotic-sensing capability of His-CDs was tested using staurosporine, an apoptosis inducer. A concentration-dependent increase in fluorescence was observed with increasing staurosporine concentrations, indicating the His-CDs' sensitivity to apoptosis. The time-dependent fluorescence increases were noted with prolonged staurosporine exposure. Z-DEVD-FMK, a caspase-3 inhibitor, confirmed that the apoptosis detected by His-CDs was caspase-3 dependent, as co-treatment reduced His-CDs' fluorescence in the cell. In conclusion, these results demonstrate that His-CDs are biocompatible, sensitive apoptosis sensors and hold the potential for monitoring apoptotic pathways in cellular systems.



SPATIAL DETERMINATION OF TUMOR CELL APOPTOSIS AND CD8+ T CELL INFILTRATION IN IN-VIVO TUMOR TISSUE SAMPLES

Derya Goksu Helvacı^{1,2}, Zhixuan (Sara) Huang^{1,2}, Kenneth Hu^{1,2}

¹Department of Immunology, ²James P. Allison Institute, The University of Texas MD Anderson Cancer Center, Houston, TX, TSA

The ultimate goal of immunotherapy is tumor control through restraint of growth and elimination of tumor cells. Determining kinetics and localization of tumor cell apoptosis and how it relates to immune cell localization

immediately following immunotherapy is crucial for understanding its failure modes. CD8⁺ T cells are often the main contributors to tumor cell elimination and their infiltration into the tumor parenchyma has been associated with better anti-tumor responses. However, the immune cell subsets most directly associated with hotspots of tumor cell killing remain uncharacterized.

Here we propose an approach that combines genetically encoded caspase reporters with large-volume tissue clearing and imaging to fully characterize the spatiotemporal dynamics of tumor cell killing post-ICB in preclinical mouse models. By leveraging advanced imaging and computational analysis, our study bridges this gap, making it possible to visualize tumor-immune interactions in-vivo.

In this study, we used the GC3AI reporter, an established method for detecting real-time apoptosis in in vitro studies². To enable detailed 3D reconstruction of individual tumor cells, including the shapes, sizes, and behaviors, we used 200 μm -thick tissue sections. Thick sections provided a unique advantage for studying tumor architecture and cell dynamics. Additionally, we applied Ce3D-based tissue clearing method, which effectively cleared and enabled imaging of the thick sections³. This method enabled effective clearing and index matching of the samples, allowing for high-resolution imaging of large tissue volumes, and enhancing our ability to visualize tumor-immune interactions (Figure 1).

To analyze the spatial relationship between CD8⁺ T cells and tumor cell apoptosis, Imaris software was used to classify individual cells. Highly apoptotic regions were identified using density-based clustering in R. CD8⁺ T cell density and locations were plotted and overlaid onto the tumor cell apoptosis density graph (Figure 2).

Our findings revealed distinct zones of apoptosis following ICB treatment with anti-CTLA4, with a weak correlation between CD8⁺ T cell density and localized apoptosis. This suggests that CD8⁺ T cell local abundance alone may not fully account for tumor cell death in these regions. Using the GC3AI reporter to detect endogenous, real-time apoptosis without the need for dyes or stains is a powerful tool for studying tumor responses. These insights lay the groundwork for future investigations into the mechanisms driving localized apoptosis and their implications for optimizing immunotherapy.

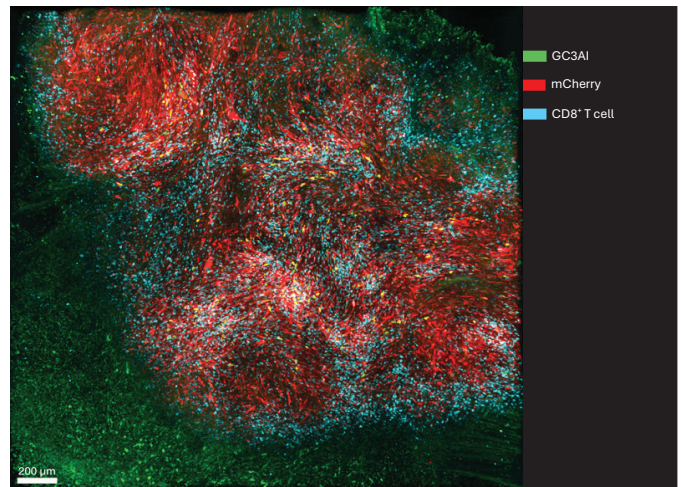


Figure 1: Visualization of tumor sections using the GC3AI reporter and Ce3D-based tissue clearing: Representative 200 μm -thick tumor section showing GC3AI (green) for apoptosis, mCherry (red) for tumor cells, and CD8⁺ T cells (cyan). Scale bar = 200 microns

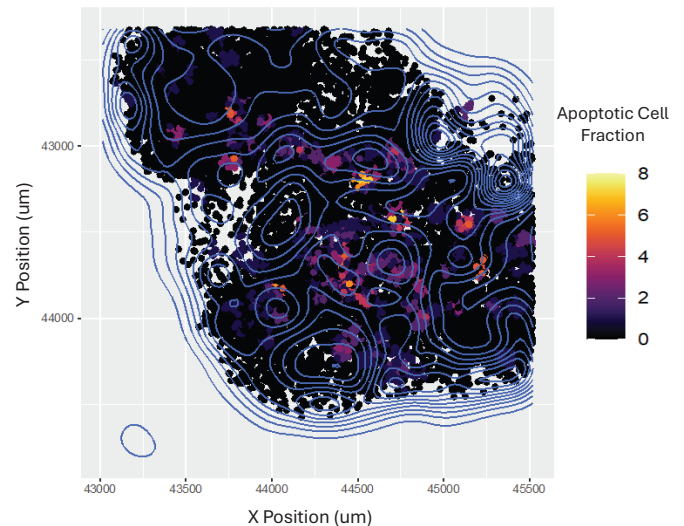


Figure 2: Computational representation of highly apoptotic regions and CD8⁺ T cell distribution: 2-dimensional reconstruction of the 200 μm -thick tumor section with local apoptotic tumor cell density denoted by spot color. CD8⁺ T cells density data was overlaid (blue contours).

References:

- 1) Raskov, H., Orhan, A., Christensen, J.P. *et al.* Cytotoxic CD8⁺ T cells in cancer and cancer immunotherapy. *Br J Cancer* 124, 359–367 (2021). <https://doi.org/10.1038/s41416-020-01048-4>
- 2) Zhang, J., Wang, X., Cui, W. *et al.* Visualization of caspase-3-like activity in cells using a genetically encoded fluorescent biosensor activated by protein cleavage. *Nat Commun* 4, 2157 (2013). <https://doi.org/10.1038/ncomms3157>
- 3) Li, W., Germain, R.N. & Gerner, M.Y. High-dimensional cell-level analysis of tissues with Ce3D multiplex volume imaging. *Nat Protoc* 14, 1708–1733 (2019). <https://doi.org/10.1038/s41596-019-0156-4>

ANTIBACTERIAL TELLURIUM DIOXIDE NANOPARTICLES

Tina Hesabizadeh¹, Rajendra Subedi¹, Thomas J. Webster^{2,3,4}, and Grégory Guisbiers^{1,*}

¹Department of Physics and Astronomy, University of Arkansas at Little Rock, 2801 South University Avenue, Little Rock, AR 72204, USA

²School of Health Sciences & Biomedical Engineering, Hebei University of Technology, China

³School of Engineering, Saveetha University, Chennai, India

⁴Division of Pre-college & Undergraduate Students, Brown University, Providence, USA

The anti-bacterial properties of tellurium dioxide nanoparticles have already been mentioned in the literature [1-3]. In our previous study [3], tellurium dioxide nanoparticles (TeO₂) were synthesized by pulsed laser ablation in liquids (PLAL) using a top-ablation set-up. However, according to Ref. [4]; smaller tellurium dioxide (TeO₂) nanoparticles can be obtained by using a bottom-ablation set-up instead of a top-down one. Therefore, in this study, TeO₂ nanoparticles were synthesized by PLAL using a bottom-ablation set-up in order to investigate the effect of size reduction on their antibacterial properties. The solvent and target were de-ionized water and pure tellurium, respectively, as in Ref. [3]. The produced TeO₂ NPs were spherical with a diameter of 56 ± 13 nm; smaller in comparison to the ones synthesized in Ref. [3]. This PLAL technique yielded nanoparticles with clean surfaces, enhancing their interactions with bacteria. The antibacterial properties were confirmed using standard bacterial culture assays, which demonstrated significant inhibitory effects on both Gram-positive and Gram-negative bacteria, specifically *Escherichia coli*, *Pseudomonas aeruginosa*, *Staphylococcus epidermitis*, and Methicillin-resistant *Staphylococcus aureus* (MRSA). The nanoparticles were further tested for biocompatibility by exposing them to fibroblast cell cultures, where no significant cytotoxic effects were observed. Additionally, the TeO₂ NPs were drop-casted onto a Band-Aid, where a significant antibacterial effect was also observed. These findings underscore the great potential of using TeO₂ nanoparticles as an antimicrobial wound care solution.

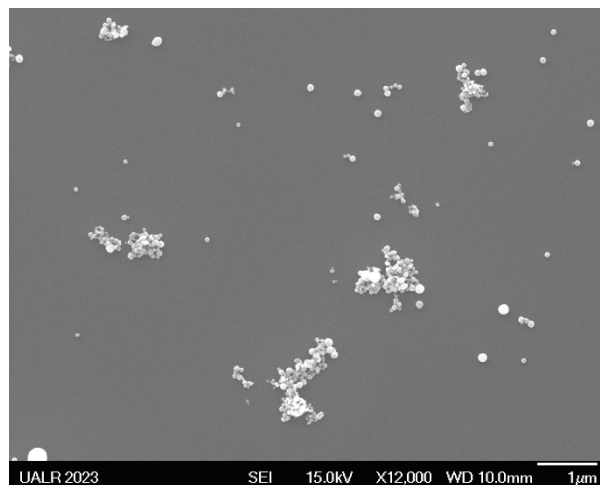


Figure 1. SEM image of the TeO₂ nanoparticles

- [1] I. N. Saraeva, E. R. Tolordava, A. A. Nastulyavichus, A. K. Ivanova, S. I. Kudryashov, A. A. Rudenko, N. N. Melnik, D. A. Zayarny, A. A. Ionin, Y. M. Romanova, S. A. Gonchukov, *A bacterial misericorde: laser-generated silicon nanorazors with embedded biotoxic nanoparticles combat the formation of durable biofilms*, *Laser Physics Letters* (2020) vol. 17, 025601.
- [2] W. K. Khalef, T. R. Marzoog, A. D. Faisal, *Synthesis and characterization of tellurium oxide nanoparticles using pulse laser ablation and study their antibacterial activity*. *J. Phys.: Conf. Ser.* 2021, 1795, 012049.
- [3] T. Hesabizadeh, E. Hicks, D. Medina Cruz, S. E. Bourdo, F. Watanabe, M. Bonney, J. Nichols, T. J Webster, G. Guisbiers, *Synthesis of "Naked" TeO₂ Nanoparticles for Biomedical Applications*, *ACS Omega* (2022) vol. 7, 23685-23694.
- [4] R. Subedi, G. Guisbiers. *Synthesis of Ultrawide Band Gap TeO₂ Nanoparticles by Pulsed Laser Ablation in Liquids: Top Ablation versus Bottom Ablation*. *ACS Omega* (2024) vol. 9, 25832-25840.

TEXTURE ANALYSIS OF LUNG CELL SURFACE MORPHOLOGY AFTER NANOPARTICLE EXPOSURE.

Taylor Jefferis¹, Akshatha Mohan², Christie M. Sayes¹, and Joshua Peeples². ¹Department of Environmental Science, Baylor University, Waco, TX, USA. ²Department of Electrical and Computer Engineering, Texas A&M University, College Station, TX, USA.

Inhalation of nanoparticles present in the air we breathe may cause discomfort of the airway and lungs. Nanoparticles that elicit this distress are classified as irritants, which cause acute discomfort of the airways, or respiratory sensitizers, which trigger a more complex hypersensitivity response and lead to long-term health

effects upon repeated exposure. This exposure may induce morphological changes to the surface of the lung cells, necessitating robust methods for quantitative analysis. Microscopy techniques provide valuable data sets for use in computer vision and other machine learning tools, to assess effects demonstrated on the cell surface, which helps elucidate possible modes of toxic action. Scanning electron microscopy (SEM) provides high-resolution images from which researchers can draw conclusions about the effects of nanoparticle exposure. Computer vision may then be used to objectively quantify and analyze the changes seen throughout multiple images.

This study provides a novel texture analysis framework that leverages fractal dimension and lacunarity analysis,

combined with a Quantized Co-Occurrence (QCO) operator and Earth Mover's Distance (EMD) to capture both local and global textural features directly from grayscale SEM images. Images of untreated cells will be compared against images of cells that have been exposed to nanoparticles that are known sensitizers, such as nickel oxide (NiO), and known irritants, such as crystalline silica (CS). This combined framework enables us to visualize and rank nanoparticle-induced effects in cell surface morphology, providing key insights into the differential impact of nanoparticles. This work will provide the framework for high-content screening (HCS) capability, combining microscopy and quantitative image analysis that can address the biological impact of contaminants.

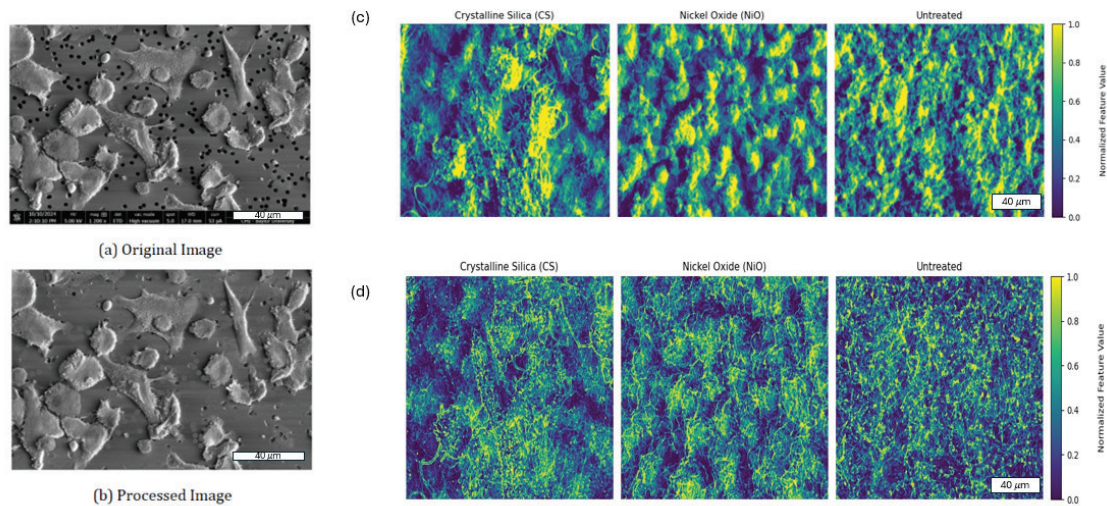


Figure 1. Steps in processing of SEM images. All scale bars represent 40 μ m. **(a-b)** Comparison of images before and after texture feature extraction by computer vision. **(c)** Average pooling feature maps showing spatial distribution across different cell exposures. **(d)** Lacunarity feature maps showing texture characteristics and morphological variations between different cell exposures.

IN VITRO IMMUNO-IMAGING OF NATURAL KILLER CELL CYTOTOXICITY IN KIDNEY CANCER

Ludovica La Posta^{1,2}, Sofia Rosy Caterina Sorice¹, Nadima Uprety³, Rafet Basar³, Hind Rafei³, Katy Rezvani³, Eleonora Dondossola¹

¹ Department of Genitourinary Medical Oncology, UT MD Anderson Cancer Center, Houston

² Rice University, Department of Bioengineering, Houston

³ Department of Stem Cell Transplantation and Cellular Therapy, UT MD Anderson Cancer Center, Houston

Renal cancer is one of the ten most frequent cancers in both women and men, with clear cell renal cell carcinoma (ccRCC) being the most common form of RCC (75% overall incidence). Treatment options for metastatic

ccRCC have evolved towards the application of immune checkpoint blockade and small molecule antiangiogenic tyrosine kinase inhibitors (TKIs), as single or combined agents. Despite unprecedented success, only a subset of patients (~30%) benefit from these treatments due to emerging resistance. Therefore, to improve patient survival, it is crucial to test new therapeutic options, including cellular immunotherapy. Natural killer (NK) cell transplantation has recently emerged as a promising off-the-shelf cell therapy due to their inherent ability to kill cancer cells without prior sensitization and without causing graft versus host disease in the allogeneic setting. However, characterization of NK cell biology is challenging, including high-throughput, high-quality, and quantitative imaging data from biologically relevant models. Furthermore, conventional in vitro studies have limited ability to assess dynamic intercellular interactions at the subcellular level, in real time. To overcome these

limitations, we established a fully human in vitro co-culture to assess the dynamics of tumor cell killing by NK cells using real-time microscopy at the subcellular level. This multicellular assay has proven useful for monitoring the dynamics of NK cell effector function, mutual interactions between tumor cells and NK cells, and quantitative measurements of NK-mediated cytotoxicity.

THE IMPACT OF ANTIANGIOGENIC THERAPY ON BLOOD VESSELS AND CD8 INFILTRATION IN RENAL CANCER METASTASES IS SPACE, TIME, SITE, DOSE, AND DRUG DEPENDENT

Stefan Maksimovic¹, Nina Costanza Boscolo¹, Matthew T. Campbell¹ and Eleonora Dondossola¹

¹ Department of Genitourinary Medical Oncology, UT MD Anderson Cancer Center, Houston, TX

Clear cell renal cell carcinoma (ccRCC) is the most prevalent renal neoplasm, with bone as a major site for distant spread in 35% to 40% of the patients. These metastases are typically osteolytic, resistant to treatments, hence result in a variety of skeletal-related complications strongly contributing to mortality. A key feature of ccRCC is the loss of function of the von Hippel-Lindau (VHL) protein leading to extensive angiogenesis. Consequently, different anti-angiogenic tyrosine kinase inhibitors (TKIs) are used as first or subsequent line of treatment for these patients as single agents or in combination with immune checkpoint inhibitors. However, limited data about their efficacy in bone metastasis is available, and their impact on the immune infiltrate, including effector CD8 cells is unclear. We hypothesized that TKIs, by inhibiting angiogenesis, significantly reprogram the microenvironment and limit immune infiltration in a space, time, dose, and drug dependent fashion.

To test these hypotheses, we developed immunocompetent mouse model of bone metastasis by orthotopic intratibial implantation of luciferase-GFP-positive mouse RENCA-VHL- cell line. Interestingly, intratibial injection gave rise to metastases in lungs, creating a unique opportunity to study two metastatic sites. Three different TKIs currently used in patients were tested and compared to control: axitinib (A), cabozantinib (C), and lenvatinib (L). Outcomes were monitored by macroscopic bioluminescence detection in vivo, 3D multiparametric spatial analysis of bones and lungs, in vivo, and ex vivo.

Compared to control-treated mice, high doses of A, C, and L significantly reduced tumor progression in both tumor sites. Even though these TKIs are clinically considered equal, significant differences in their efficacy were noted. Spatial analysis of tumor cells and blood vessels showed a significant decrease in blood vessels formation in both an organ- and TKI-specific pattern over time. Additionally, the reduction of neoangiogenesis in treated tumors directly limited the infiltration of CD8 cells, which localized at the interface with tumor free bone/lung tissue. Interestingly, TKI dose reduction significantly improved CD8 infiltration, while controlling tumor size. TKI withdrawal, instead, led to rapid progression of tumor in both sites and significantly shortened mice survival.

In conclusion, we established bone and lung metastatic models of ccRCC, and characterized and compared the effects of three antiangiogenic TKIs on angiogenesis and CD8 infiltration. TKIs reduced tumor growth and progression, as a consequence of blood vessel formation inhibition. Furthermore, TKI treatment reduced the infiltration of effector T cells in tumors in a dose-dependent manner, an outcome that can have a major impact when TKIs are combined with immunotherapy, a preferential therapeutic regimen for ccRCC patients. Overall, we believe our studies provide important insights and efficacy predictions for innovative therapeutic applications in ccRCC bone metastatic patients.

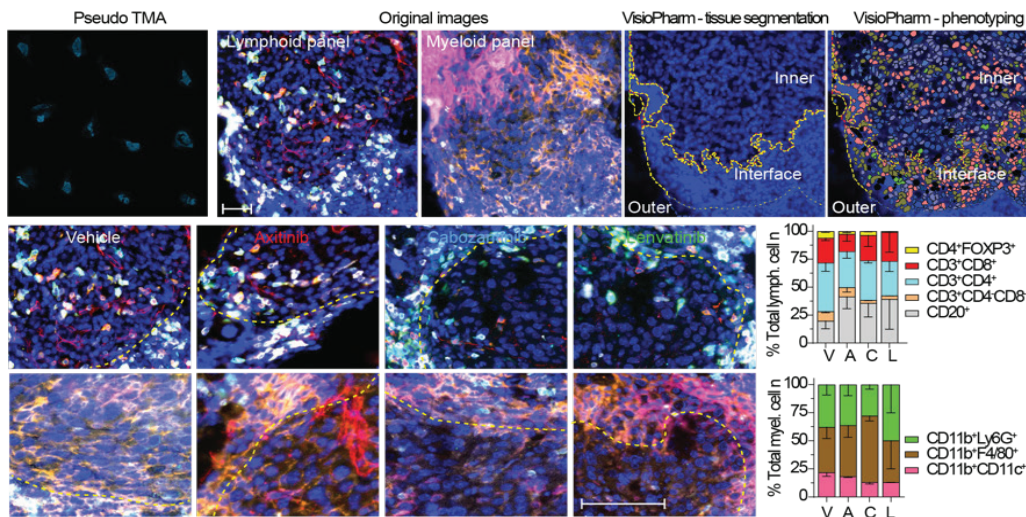


Figure 1. COMET multiplex analysis (CMA). CMA was applied to study the impact of TKIs on immune cell distribution in tumor infiltrating bone marrow. All scale bars are 100 μ m.

CHARACTERIZATION OF NEMATODE POPULATIONS WITHIN HADROSAUR BONES AT HELL CREEK, MONTANA USA.

Kersten A. Peterson, Mark H. Armitage, DSTRI.org, Sequim, WA, 98382.

Samples taken from the partially permineralized bone and ossified tendons of the hadrosaurid dinosaur, *Edmontosaurus annectens*, (and other Cretaceous dinosaurs) found at the Hell Creek Formation (Montana and eastern Wyoming,) and the Maastrichtian Hell Creek Formation in South Dakota have yielded stunningly preserved soft tissue structures including osteocytes and blood vessels [1, 2, 3, 4], collagenous matrix [1, 4] and nerves [5]. However, endogenous soft tissue structures are not the only microscopic finds being reported. Evidence of microorganisms including nematodes, fungi (or the evidence thereof) and helminth eggs have been found in vessel canals, gut remains, and coprolites from multiple hadrosaurid dinosaur specimens [6, 7, 8]. The discovery of microscopic organism communities in dinosaur remains is rare and provides important records of relationships between soft-bodied invertebrates and the remains of dinosaur bone and gut material. Many studies reporting helminths associated with extinct animal remains including two of the hadrosaurid reports cited here, argue that these microorganisms were endemic parasitic infestations and were preserved at death. However, some studies suggest that these helminth populations may instead be from opportunistic extant worms living in and gaining nutrients from the preserved remains [6]. In the present study, we present an analysis of populations observed in *E. annectens* from Hell Creek, MT, and provide evidence that these nematodes are opportunistic extant fungivores rather than parasites. Nematode adult and juvenile population counts were analyzed under

brightfield from 40um ground sections of *E. annectens* scapula and jaw (Figure 1). The orientation of the worms suggests this population was feeding on fungus growing on decaying soft tissues (or possibly residual tissue) within bone canals at the time of collection and emplacement in fixative. To characterize live nematode populations in bones and in soil surrounding bones in Montana, a field adapted Baermann funnel technique allowed us to collect, identify, and analyze worm populations. One living fungivorous nematode was extracted from a triceratops bone shard (Figure 2). Resulting species identification and population dynamics were compared with the nematode populations observed in the *E. annectens* bone sections.

References

1. PV Ullmann, *et al*, *Cretaceous Research*, 99 (2019), p. 1-13. DOI: <https://doi.org/10.1016/j.cretres.2019.02.012>
2. MH Armitage and KL Anderson, *Acta Histochemica* 115 (2013), p. 603-608. DOI: <http://dx.doi.org/10.1016/j.acthis.2013.01.001>
3. MP Guilliams, *The Research and Scholarship Symposium*, 49, Microstructures Produced by Hadrosaur Bones from Alaska and Wyoming. https://digitalcommons.cedarville.edu/research_scholarship_symposium/2016/poster_presentations/49/
4. MH Armitage, *Microscopy Today*, 24(1) (2016), p. 18-22. DOI: <https://doi.org/10.1017/S155192951500113>
5. MH Armitage, *Microscopy Today* 29(2) (2021), p. 20-25. DOI: <https://doi.org/10.1017/S1551929521000468>.
6. MH Armitage, *Microscopy Today* 32(1), 2024, p. 26-34. DOI: <https://doi.org/10.1093/mictod/quaad110>.
7. J Tweet, *Journal of Paleontology*, 90(2) (2016), p. 279-287. DOI: <https://doi.org/10.1017/jpa.2016.43>
8. G Poinar, *Parasitology*, 133(2) (2006), p. 245-249. DOI: <https://doi.org/10.1017/S0031182006000138>

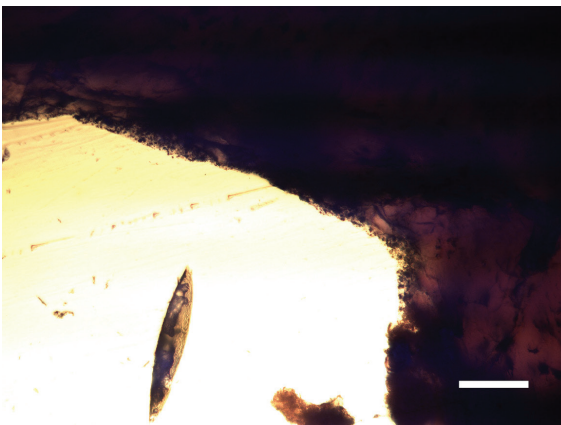


Figure 1: Nematode in blood canal, *Edmontosaurus* jaw, Glendive, MT. Scale bar = 100µm.

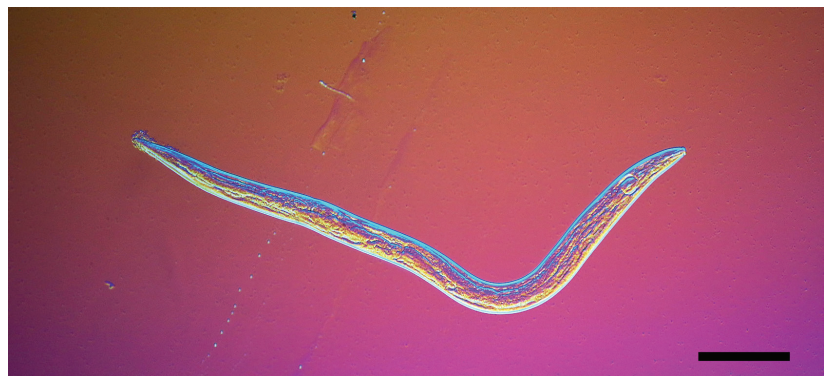


Figure 2: Living fungivorous nematode, extracted from Triceratops buried shard, Glendive, MT, scale bar = 90 µm.

TRACKING OF NANOPARTICLE TRANSFERRIN- DERIVED CARBON DOTS FOR TARGETED THERAPEUTICS

Sara Strickland, Hamed Faleke, Adyson Alexander,
and Dimitri Pappas

Department of Chemistry and Biochemistry, Texas Tech
University Lubbock, TX 79409-1061

Our previously reported transferrin-derived carbon dots (Tf-CDs) have demonstrated retained protein function by selectively binding to the cancer biomarker and transferrin receptor, CD71. Utilizing super-resolution radial fluctuation (SRRF) microscopy, the Tf-CDs were observed to enter the cells in small vesicles approximately 100 nm in diameter, then accumulating inside the cell, suggesting the clathrin-coated pit uptake pathway commonly utilized by transferrin upon binding to CD71 was responsible. Particle tracking via TrackMate indicated active nanoparticle uptake and accumulation within organelles. Colocalization analysis determined that the nanoparticles entered the cell via early endosomes than then acidified into late endosomes which then fused to lysosomes within minutes. These results matched the degradation pathway of transferrin, not the recycling pathway of transferrin. This means that the Tf-CDs are confined within the cell and not recycled back out in the extracellular space. This uptake and confinement property is a highly desired trait for nanoparticles for certain applications, such as targeted therapeutics. To test this, we then conjugated Tf-CD to staurosporine, a compound which acts as a protein kinase inhibitor which can induce apoptosis in a variety of cells. Compared to 10 μM staurosporine alone, 10 μM of the Tf-CD staurosporine conjugate incubated in CD71 expressing human leukemia cells for 6 and 3 hours exhibited a 1.3x and 2.2x increase in cell death, respectively. These results indicate that due to Tf-CDs ability to selectively target, enter, and accumulate within malignant cells via over expression of CD71, these CDs can be conjugated with a variety of cancer killing agents improving the therapeutics selectivity and efficacy.

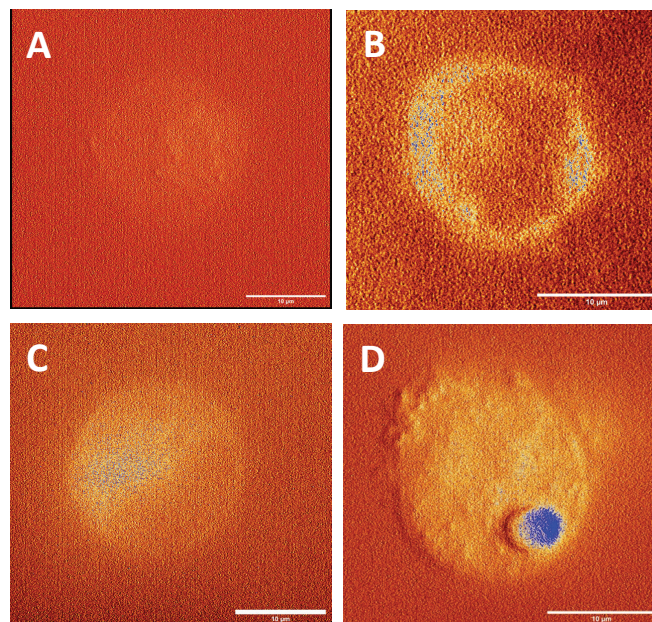


Figure 1. HL60 cell line of promyeloblast cells isolated from a patient with acute promyelocytic leukemia cell line) imaged under 466/40 nm bandpass filter. SRRF microscopy images with (A) no staining agent, (B) 26 μM Tf-CDs after 0 min incubation, (C) 3 min incubation, and (D) 5 min incubation. Bars=10 μm .

ELECTRON MICROSCOPY REVEALS CADMIUM-INDUCED ULTRASTRUCTURAL ALTERATIONS IN YEAST CELLS.

Sunday Olaniyan¹, Bernd Zechmann^{1,2}, Bessie Kebaara¹.
¹Department of Biology, Baylor University, Waco Texas,
76798

²Center for Microscopy and Imaging, Baylor University,
Waco Texas, 76798

Understanding how cells adapt to heavy metal stress is critical for uncovering mechanisms of toxicity and detoxification. This study used Transmission Electron Microscopy (TEM) and Scanning Electron Microscopy (SEM) to investigate the ultrastructural features of *Saccharomyces cerevisiae* (yeast) cells exposed to cadmium stress, comparing them with unexposed controls. TEM, a high-resolution imaging technique, was employed to analyze structural changes at the subcellular level. Various yeast strains with differing capacities to pump out cadmium were analyzed to evaluate their tolerance and ultrastructural responses. For sample preparation, high-pressure freezing (HPF) was utilized to preserve cellular architecture with minimal artifacts. Unlike traditional chemical fixation, HPF avoids the use of water and fixes samples in milliseconds, preventing potential dilution and re-distribution of intracellular cadmium and ensuring accurate visualization of metal-induced structural changes. TEM and SEM analysis revealed prominent structural alterations in cadmium-exposed

cells, notably the enlargement of vacuoles, which play a critical role in cadmium sequestration and detoxification (Fig. 1A, B). Additional observed changes include the dilation of the endoplasmic reticulum, and cell wall distortions, highlighting the impact of cadmium stress on cellular structure (Fig 1B). In contrast, unexposed control cells display intact organelles and well-preserved ultrastructure, providing a baseline for comparison (Fig 1A). SEM investigations revealed distorted physical appearance on the cells exposed to cadmium, while the control and unexposed cells had no impact. By revealing the structural adaptations and stress-induced damage in yeast cells, this work contributes to a broader understanding of cadmium toxicity and the cellular mechanisms that underlie detoxification processes. Such insights could inform future studies aimed at mitigating the effects of heavy metal stress in biological systems.

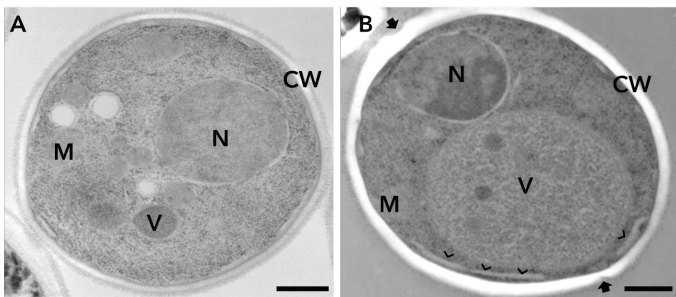


Figure 1: TEM micrographs showing yeast cells grown in cultures (A) without cadmium (control), and (B) with 50 μ M cadmium. Cadmium treated cells show large vacuole (V), dilated ER (arrowheads), and thicker and distorted (arrows) cell walls (CW). M=Mitochondria, N= Nuclei. Bars= 500nm.

BIOMECHANICAL CHANGES IN THE BRAIN OF CEREBRAL AMYLOID ANGIOPATHY. Alexis Mack¹, Caroline Reynolds¹, Hannah Thompson¹, Travis Moore², Sean Marrelli¹, Akihiko Urayama¹. Department of Neurology¹, Department of Integrative Biology and Pharmacology², University of Texas Medical School at Houston, Houston Texas 77030.

Cerebral amyloid angiopathy (CAA) is common in Alzheimer’s disease (AD) patients. CAA affects approximately 82–98% of AD patients on autopsy and is associated with an increased burden of cerebrovascular insults, affecting the leptomeningeal and cortical arteries, arterioles, and capillaries with the deposition of aggregated amyloid-beta ($A\beta$), a hall mark of AD pathology. CAA impairs cognitive function

via multiple mechanisms, including progressive impairment of brain clearance of $A\beta$, reduced neurovascular coupling, dysregulation of blood brain barrier (BBB), as well as lobar intracerebral hemorrhage which is caused by cerebrovascular leakage. Thus, the present study investigates how biomechanical changes in the brain of CAA-laden blood vessels affect the integrity of BBB through mechanosensitive signals. We employed CAA model TgSwDI mice at 16 months of age, showing progressive cortical amyloidosis and capillary CAA (type 1). Fluorescence-guided atomic force microscopy (AFM) was employed to determine the local Young’s elastic modulus (YM) of brain tissue from the somatosensory cortical layer III/IV in TgSwDI and wild-type (WT) mice. In Fig. 1, regional tissue stiffness was estimated by force-volume mapping by AFM in the somatosensory cortical layer III/IV in TgSwDI and WT control mice. While MX04-positive vascular $A\beta$ aggregates showed excessive stiffness (>176 kPa), the stiffness of cortical tissue in WT and TgSwDI mice ranged 0.6-2.0 kPa and 0.07-4.46 kPa, respectively. The average brain stiffness in TgSwDI mice was 2.01-2.62 fold softer than that of age-matched WT mice (1.37 kPa), suggesting increased regional heterogeneity in stiffness of the capillaries in TgSwDI mice, while the stiffness of brain tissues in WT mice was relatively uniform. The present study suggests that CAA-laden blood vessels were surrounded by softer substrates which may compromise BBB integrity.

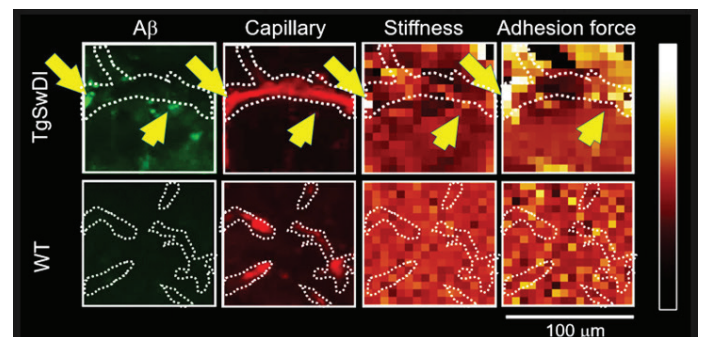


Fig. 1. Increased regional heterogeneity in the tissue stiffness and adhesion force in CAA laden blood vessels in aged TgSwDI mice. AFM Force/volume maps in the cerebral cortex in 16 months old TgSwDI mice were shown. Arrows indicate the location of $A\beta$ deposition. $A\beta$: MX04 (10 mg/kg) Blood vessel: Tomato lectin-AF649.

VISUALIZATION OF LIPOSOMES WITH A MODIFIED IMAGING TECHNIQUE USING ATOMIC FORCE MICROSCOPY.

Ana Maria Zaske

Internal Medicine, Cardiovascular Medicine. UT Health Science Center at Houston. 77054.

Nano-biotechnologies represent an unprecedented recent advance that may revolutionize many areas of medicine and biology. We are now able to evaluate the effects of a treatment in cancer cells, analyze the efficiency of skin healing or just simply observe DNA structures, all at the nano-metric scale. Atomic force microscopy (AFM) is a surface technique that generates nanoscale analytical data under physiological-like conditions. Combined with fluorescence microscopy, AFM is an attractive tool for characterizing nanoparticle-cell membrane interactions and may afford the opportunity to image biological processes in real time. Nevertheless, structure recognition can be a challenge during AFM imaging. Some nanoparticles can be used as imaging contrast agents and as reinforcement elements to improve visual enhancement [1]. Colloidal gold has excellent detection capabilities for single-molecule tracking [2]. The aim of this project was to standardize the use of gold nanoparticles as a nontoxic means to detect pegylated liposomes by AFM.

The corrugated surface of the cell membrane sometimes hinders the visualization of extracellular entities that may interact with the cell. To overcome this barrier, we used 90 nm nanogold particles to label FITC liposomes and monitor their endocytosis on human coronary artery endothelial cells (HCAECs). We successfully visualized the internalization process of gold-coupled liposomes *in vitro*.

We found that the gold-liposomes attached to the HCAEC cell membrane during the first 15–30 min of incubation, liposome cell internalization occurred from 30 to 60 min (**Figure 1**), and most of the gold-labeled liposomes invaginated after 2 hr of incubation. Liposomal uptake took place most commonly at the periphery of the nuclear zone. This study showed the versatility of the AFM technique, combined with fluorescent microscopy, for investigating liposome uptake by endothelial cells for medical applications. The 90 nm colloidal gold nanoparticles proved to be a noninvasive contrast agent that efficiently enhanced AFM imaging during the investigation of biological nano-processes.

New insights have developed, in the AFM field, to determine the elastic properties of biological materials. We routinely estimate the Young's Modulus of cells and fresh tissues to help to understand the mechanisms of several physiological processes, such as differentiation, growth, drug treatment, and disease [3], [4]. Additionally, it is possible to map the distribution of elastic responses

on the sample surface by combining force curve measurements with topographic imaging. Examples of the accomplishments using the AFM technique in several of our projects will be briefly mentioned during our talk. The unique properties of AFM offer unlimited applications in medical research. It can provide valuable insights about the mechanisms of a disease, and assess a successful treatment pathway for its cure.

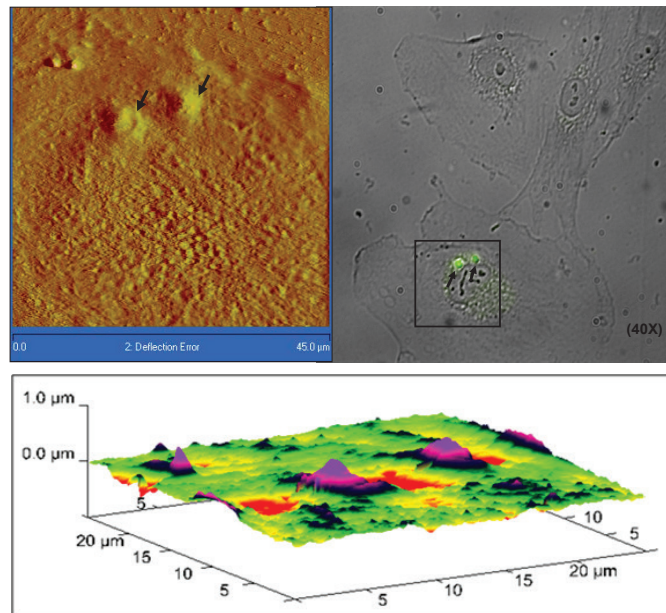


Figure 1. - AFM and fluorescence images of gold labeled liposomes during the membrane internalization process occurring after 60 min of incubation in HCAEC's. AFM scanning in liquid using contact mode and DNP-S cantilevers ($f_0 = 12\text{--}24\text{kHz}$, $k = 0.06\text{N/m}$).

REFERENCES:

- [1] LUDERER, F.; K. STERNBERG *et al.* (2008). "Suitability of nanoparticles for stent application," in *Proceedings of the 4th European Conference of the International Federation for Medical and Biological Engineering (ECIFMBE '08)*, vol. 22, pp. 2339–2342.
- [2] HAINFELD, J. F. and R. D. POWELL (2000). "New frontiers in gold labeling." *Journal of Histochemistry and Cytochemistry*, vol. 48, no. 4, pp. 471–480.
- [3] LEE, SEI-YOUNG; ANA-MARIA ZASKE; TOMMASO NOVELLINO; DELIA DANILA; MAURO FERRARI; JODIE CONYERS; PAOLO DECUZZI (2011). "Probing the mechanical properties of TNF- α stimulated endothelial cell with atomic force microscopy". *International Journal of Nanomedicine* 6: 179–195, 2011. PMID: 21499414.
- [4] COPELAND, IAN; ANA M. ZASKE *et al.* (2024). "Exome sequencing implicates ancestry-related Mendelian variation at SYNE1 in childhood-onset essential hypertension". *JCI Insight* 9 (9): e172152. PMID: 38716726.

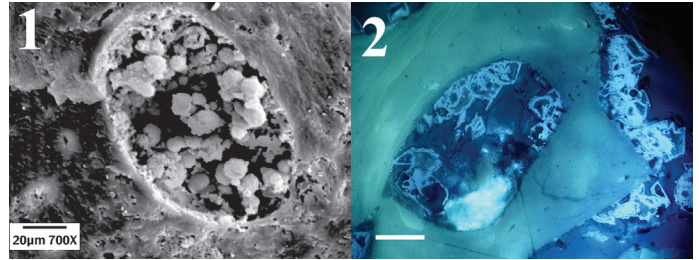
LIGHT AND ELECTRON MICROSCOPE STUDIES OF IRON OXIDE FRAMBOIDS IN VESSELS OF DINOSAUR BONES.

Mark H. Armitage, Keith Holcomb, Kersten Peterson, DSTRI.org, Sequim, WA, 98382.

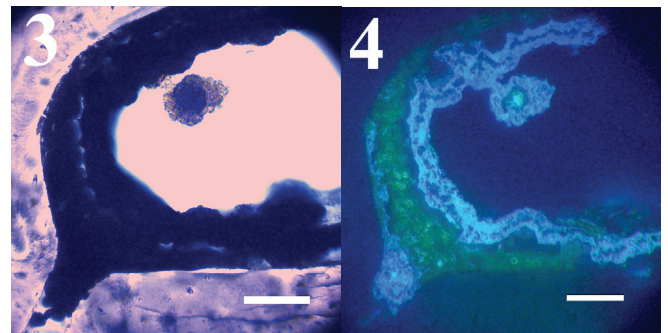
The findings of soft tissue in dinosaur bones remain controversial, yet reports of soft tissue continue to be made [1, 2, 3]. To date, approximately 140 individual dinosaur bones have been demineralized (and reported) specifically for the purpose of collecting and characterizing soft tissues that might remain within them [1].

We collected *Edmontosaurus* post-cranial limb elements at Hell Creek Formation in Glendive, MT, USA, and limb bone elements from *Camarasaurus* at the Morrison Formation in CO, USA. Bones were subjected to fixation in formalin at the site for transport to the lab. Bones were rinsed in pure water, air-dried and ground thin sections were made to 40 micron thickness, Sections were affixed to glass slides and were examined without coverslip under reflected light UVFL for the presence of auto-fluorescing framboids within microvascular bone canals. Framboids are microscopic (about 20 μ m in diameter) spherical aggregates of iron oxide or iron-pyrite, common in sedimentary layers and often found in dinosaur bone canals. Sections were also imaged under both secondary and backscattered electrons. Framboids were identified as spheres of varying sizes (Figures 1, 2). Elemental analysis revealed a substantial presence of iron and oxygen in framboids. Bones were also subjected to decalcification in EDTA and vessels with framboids within them were photographed in brightfield and UVFL microscopy. All framboids auto-fluoresced brightly under UV illumination indicating massive presence of iron-probably from heme in blood, especially *Edmontosaurus* (Figure 2) and *Camarasaurus* (Figure 4). Despite deep-time environmental factors, (erosion, water infiltration, annual freeze-thaw cycle, radiation) and predation (by bacteria, fungi, microbes, insects and worms), framboids adhered tenaciously within bone matrix walls and often completely occluded blood canals for the entire depth of sections (Figure 2). We were stunned that fixation, washing, dehydration and mechanical vibration (during intense grinding for sectioning), did not dislodge framboids or even separate them from canal walls. They form tight and uniform junctions against the hydroxyapatite walls

of bone they are lodged in. Framboids are present in Volkmann canals as well. Intrusion of calcite or silica were not observed under polarized light. Many reports of putative blood cells have been made in the dinosaur soft tissue literature [4, 5], however as we have shown here, these structures are the wrong size and shape for red blood cells or white cells. They vary greatly in size but are present as round spheres, composed mostly of iron oxide.



Figures 1,2 SEM and UV Fluorescence (UVFL) framboids in *Edmontosaurus* limb microvascular canal, 40 micron ground section (Figure 2).



Figures 3,4 Brightfield (BF) and UV Fluorescence (UVFL) framboid in *Camarasaurus* limb microvascular canal, 40 micron ground section.

References

1. PV Ulman and MH Schweitzer, *Palaios* **38**(5) (2023), p. 246-257 DOI: doi.org/10.2110/palo.2022.026.
2. LA Anderson, *Earth Science Reviews* **240** (2023), 104367 DOI: <https://doi.org/10.1016/j.earscirev.2023.104367>.
3. JA Cruz and MH Armitage, *Microscopy and Microanalysis Conference Proceedings* (2024), <https://doi.org/10.1093/mam/ozae044.998>.
4. MH Schweitzer, *Scientific American* **303** (2010), DOI: <https://www.jstor/stable/26002305>.
5. AK Huttenlocker and CG Farmer, *Current Biology* **27** (2017), DOI: <http://dx.doi.org/10.1016/j.cub.2016.10.012>.

SYNTHESIS AND MICROSTRUCTURAL ANALYSIS OF Bi₂Se₃ QUANTUM DOTS

Matthew Burningham¹, Rajendra Subedi¹, Francisco Ruiz-Zepeda², Qiaohui Zhou³, Xin Lu³, Grégory Guisbiers^{1*}

¹ Department of Physics and Astronomy, University of Arkansas at Little Rock, 2801 South University Avenue, Little Rock, AR 72204, USA

² Department of Material Chemistry, National Institute of Chemistry, 19 Hajdrihova, Ljubljana 1000, Slovenia

³ Department of Physics and Engineering Physics, Tulane University, New Orleans, LA 70118, USA

Bismuth selenide (Bi₂Se₃) is an important binary compound made of a post-transition metal, bismuth (Bi, from group V), and a chalcogenide element, selenium (Se, from group VI). Indeed, it is a 3D topological insulator and thermoelectric material. In this project, strongly confined Bi₂Se₃ quantum dots (QDS) were synthesized by Pulsed Laser Ablation in Liquids (PLAL) using a top-ablation synthesis protocol [1]. Acetone was used as a solvent and the repetition rate was fixed at 1 kHz. The Bi₂Se₃ quantum dots were characterized by Dynamic Light Scattering (DLS), Transmission Electron Microscopy (TEM), Energy Dispersive X-ray Spectroscopy (EDXS), X-ray Diffraction (XRD), Raman Spectroscopy and UV-visible Spectroscopy. The diameter and the energy band gap of Bi₂Se₃ QDs were determined to be around $\sim 7\pm 3$ nm and $\sim 1.97\pm 0.19$ eV respectively.

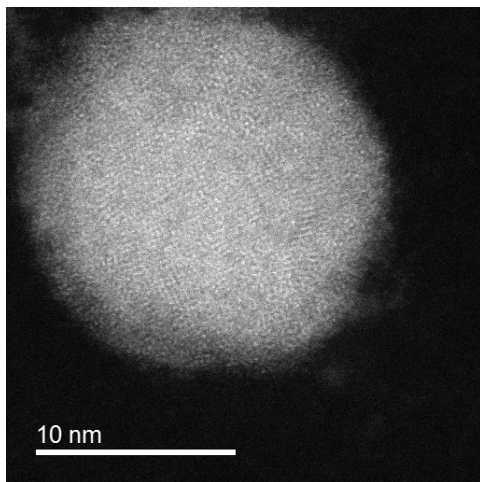


Figure 1. TEM image of a Bi₂Se₃ quantum dot.

- [1] R. Subedi, G. Guisbiers. *Synthesis of Ultrawide Band Gap TeO₂ Nanoparticles by Pulsed Laser Ablation in Liquids: Top Ablation versus Bottom Ablation*. ACS Omega. 2024;9(24):25832-25840.

BAND DISCONTINUITY STUDY OF ULTRA-WIDE BANDGAP ϵ -(In_xGa_{1-x})₂O₃/AlN

Anna Collingwood¹, Maria Sultana², and Ariful Haque^{1,2}

¹Electrical Engineering, Ingram School of Engineering, Texas State University, San Marcos, TX 78666 USA

²Materials Science, Engineering & Commercialization Program, Texas State University, San Marcos, TX 78666 USA

The excellent electronic properties of Gallium Oxide (Ga₂O₃), including an ultrawide bandgap (UWBG) of 4.9 eV, a large breakdown voltage of 8 MV/cm, and a high Baliga's figure of merit of 3214, have made it highly desirable for the next-generation high-power electronic devices¹. This groundbreaking material is poised to revolutionize critical high-power, harsh-condition technologies including electric vehicles, satellites, power transmission systems, spacecrafts, radar systems, and many more. Originally the monoclinic β -Ga₂O₃ was the most researched phase of Ga₂O₃ among its five known polymorphs due to being the most thermodynamically stable phase. The incorporation of Indium (In) in Ga₂O₃ provides the added advantage of bandgap tunability within a large range of 3.8 eV to 4.9 eV which results in excellent flexibility in electronic property tuning. In recent times, the hexagonal ϵ -Ga₂O₃ attracted significant attention owing to its highly symmetrical crystal structure and more efficient device manufacturing. Hence, ϵ -(In_xGa_{1-x})₂O₃ stood out as a promising material with its bandgap tunability and easy processing, making it ideal for next-generation high-power devices. Furthermore, a heterojunction with another UWBG material AlN can further improve the versatility of the highly sought-after ϵ -(In_xGa_{1-x})₂O₃. The implementation of AlN works as a good heat dissipator for ϵ -(In_xGa_{1-x})₂O₃ because of its relatively high thermal conductivity of 321 W/m-K. Moreover, AlN can be utilized as a gate dielectric as well as a lattice mismatch buffer layer for ϵ -(In_xGa_{1-x})₂O₃ when grown on Si. This structure ensures the high electronic performance of ϵ -(In_xGa_{1-x})₂O₃-based devices and high crystal quality epitaxial growth of ϵ -(In_xGa_{1-x})₂O₃ thin films.

For any thin film heterojunction, the carrier transport properties at the interface are largely dependent on the electronic band discontinuities at the heterointerface. As predicting carrier transport at the interface is vital for designing and implementing electronic devices, understanding band discontinuity of ϵ -(In_xGa_{1-x})₂O₃/AlN heterojunction is of crucial importance. This research focuses on the conduction and valence band offset evaluation of a ϵ -(In_xGa_{1-x})₂O₃ (x=15%) and AlN heterojunction. The ϵ -(In_{0.15}Ga_{0.85})₂O₃ was deposited by pulsed laser deposition (PLD) technique on AlN grown via metal-organic chemical vapor deposition (MOCVD)

on Si substrate. The band offsets were evaluated via the X-ray photoelectron spectroscopy (XPS)-based method developed by E.A. Kraut in 1980². A key assumption of Kraut's method is the heterojunction interface must be atomically flat.

Figure 1 illustrates a transmission electron microscopy (TEM) image of as-grown ϵ -(In_{0.15}Ga_{0.85})₂O₃/AlN/Si. The image also shows the sputter-coated carbon (C), and ion beam deposited platinum (Pt) on ϵ -(In_{0.15}Ga_{0.85})₂O₃ to prevent charging effect and film loss while preparing the TEM sample via focused ion beam. From the TEM image, it is evident that the perceived roughness at the ϵ -(In_{0.15}Ga_{0.85})₂O₃ and AlN interface is far from being atomically flat. The interface between AlN and ϵ -(In_{0.15}Ga_{0.85})₂O₃ had large peaks and valleys which is not acceptable for the Kraut's method. The peaks and valleys could have resulted in faulty band offset calculations via the Kraut's method. Hence, the high perceived roughness AlN/Si templates were disregarded and industrially grown AlN/sapphire wafers were utilized with a surface roughness of <1 nm. The final conduction band offset (CBO) was calculated to be 1.7 eV whereas the valence band offset was 0.03 eV at ϵ -(In_{0.15}Ga_{0.85})₂O₃/AlN interface. The obtained CBO for as-grown ϵ -(In_{0.15}Ga_{0.85})₂O₃/AlN heterojunction is significantly higher compared to the previously reported similar heterojunctions with CBO of 1.04 eV³ and 1.4 eV⁴. This substantial improvement indicates that electronic devices based on ϵ -(In_{0.15}Ga_{0.85})₂O₃/AlN will drastically reduce electron leakage loss, leading to exceptionally energy-efficient, high-power devices.

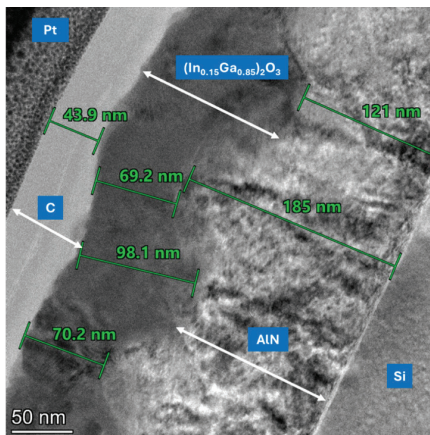


Figure 1 Thickness of as-grown ϵ -(In_{0.15}Ga_{0.85})₂O₃ and AlN on Si substrate

TEM image credit: Dr. Jonathan Anderson, Postdoctoral Scholar, Department of Physics, Texas State University

REFERENCES

- ¹ D. Araujo *et al.*, *Materials* 14(22), 7081 (2021).
- ² E.A. Kraut *et al.*, *Phys. Rev. Lett.* 44(24), 1620–1623 (1980).
- ³ S. Krishna *et al.*, *Appl. Surf. Sci.* 599, 153901 (2022).
- ⁴ A.F.M.A.U. Bhuiyan *et al.*, *J. Vac. Sci. Technol. A* 40(6), 062704 (2022).

TAILORING STRUCTURAL CHARACTERIZATIONS OF NANOMATERIALS BY TRANSMISSION ELECTRON MICROSCOPY

Guanhui Gao^{1,2}, Shaocheng Shen¹, Markus Schultz², Lars Nicolai², Gabriele Calabrese^{2,3}, Luna Esperanza², Sergio Fernández-Garrido^{2,4}, Oliver Brand², Lutz Geelhaar², Yimo Han¹, Achim Trampert²

¹Electron Microscopy Core, University of Houston, 4218 Martin L. King Blvd, 77204, Houston, Texas, USA.

²Paul-Drude-Institut für Festkörperelektronik, Leibniz-Institut im Forschungsverbund Berlin, Hausvogteiplatz 5-7, 10117, Berlin, Germany

³CNR-IMM Section of Bologna via Gobetti 101, 40129, Bologna, Italy

⁴Grupo de Electronicay Semiconductores, Dpto. Física Aplicada, Universidad Autónoma de Madrid, 28049 Madrid, Spain

Corresponding Email: Guanhui Gao, ggao7@central.uh.edu

Undoubtedly, ex-situ and in-situ (scanning) transmission electron microscopy ((S)TEM) is a versatile and powerful tool to characterize nano-materials with atomic resolution, understanding their microstructure including grain boundaries, line or point defects, structural distortions, i. e., the correlation between structure and property. Herein, various nano-structural materials are investigated via STEM techniques, which offer insights to characterize and analysis of the correlation between structure and property. For instance, GaN nanowires (NWs) can be synthesized on substrates such as metallic thin films or multilayer graphene shown in Figure 1. These metallic substrates offer attractive advantages compared to conventional substrate materials, particularly, a high electrical conductivity allowing, for example, the formation of buried contacts. However, the direct growth of inorganic semiconductors on metallic surfaces is challenging due to interfacial reactions. Here, we use sputtered Ti films on Al₂O₃(0001) and multilayer graphene on SiC(000-1) as substrates for vertically aligned GaN nanowires prepared by molecular beam epitaxy (MBE).

The major goal of the present study is to study the interface structure between the nanowires and the respective substrates and to explore its role for nanowire alignment and strain relaxation processes. Cross-sectional specimens for transmission electron microscopy (TEM) are prepared in order to examine the microstructure and chemistry of the interface. One of the key challenges of specimen preparation is to avoid contamination or chemical reactions during the samples' milling, polishing and thinning process, thus maintaining the original as-grown interface structure. High-resolution and analytical TEM,

energy dispersive x-ray spectroscopy (EDX) and electron energy-loss spectroscopy (EELS), were performed in Titan microscopes operating at 300 kV. EDXS maps and EELS scans demonstrate the incorporation of N in the upper region of the Ti film, resulting in the formation of a thin but continuous TiN layer. High-resolution (scanning) dark-field and bright-field TEM images reveal that the hexagonal GaN NWs are epitaxially aligned to the single crystalline cubic TiN layer with an orientation relationship of (111) TiN || (0001) GaN and [110] TiN || [1120] GaN showing in Figure 2. The interface is characterized by the presence of nano-twins and edge-type dislocations as a result of the large mismatch in lattice constants between GaN and TiN of about 6.4%.

Despite the expected existence of only weak van der Waals bonds between the GaN NWs and multilayer graphene, an x-ray diffraction analysis revealed the existence of a strict epitaxial relation between the NWs and the substrate. This is possibly a consequence of the damage and etching of multilayer graphene during exposure to the N plasma used for GaN NW growth, which likely introduces dangling bonds at the graphene surface. The interface is characterized by the absence of localized misfit dislocations and the first GaN layer already exhibits its relaxed bulk lattice constant. Our study demonstrates that both TiN films and multilayer graphene are promising substrates for the fabrication of vertically aligned GaN NWs on materials with metallic conductivity.

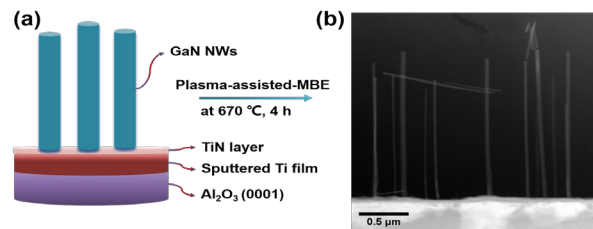


Figure 1. (a) schematic of GaN nanowires growth on sputtered Ti film via plasma-assisted MBE method, (b) low magnification HAADF-STEM image of GaN nanowires growth on sputtered Ti film.

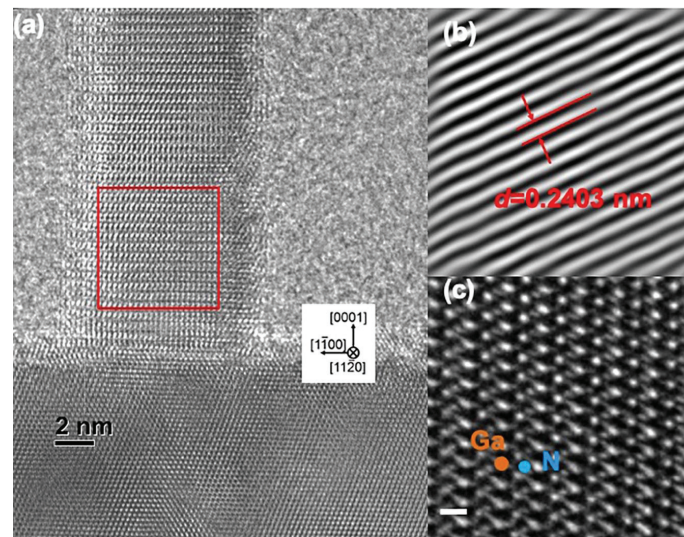


Figure 2. (a) High-resolution TEM image of GaN nanowires growth on TiN, insert of the electron diffraction pattern of GaN nanowire, (b) [1120] Bragg filtered image of the of GaN single nanowire (red-squared area in image (a)), the spacing distance of 0.2403 nm, (c) atomic resolution image of GaN single nanowire, with scale bar of 1 nm.

SYNTHESIS AND MICROSTRUCTURAL ANALYSIS OF BiSb NANOPARTICLES.

M. Khadka¹, R. Subedi¹, Joelin Ayimaa Agyei-Mensah², M. José-Yacamán², G. Guisbiers¹

¹Department of Physics & Astronomy, University of Arkansas at Little Rock, 2801 S. University Ave., Little Rock, AR 72204, USA

²Department of Applied Physics and Materials Science, Northern Arizona University, 527 S Beaver St, Flagstaff, AZ 86011, USA.

Bismuth antimonide (BiSb) was the first experimentally observed 3D topological insulator; consequently, opening new perspectives in nano-electronics [1]. In this project, BiSb nanoparticles were synthesized for the first time by Pulsed Laser Ablation in Liquids (PLAL). A nanosecond Nd:YAG laser operating at 1064 nm was used to irradiate a BiSb target totally immersed in acetone. The target was irradiated from underneath the container (bottom-ablation set-up) for 5 minutes at 1 kHz. Advanced characterization techniques such as Dynamic Light Scattering (DLS), X-ray diffraction (XRD), scanning/transmission electron microscopy (S/TEM) and energy-dispersive X-ray spectroscopy (EDXS) were performed for morphological and structural analysis. The nanoparticles were found to have a spherical shape with an average size of approximately 10 nm. Furthermore, optical properties were analyzed by using UV-visible spectroscopy, and the energy bandgap was determined to be around 2.6 eV.

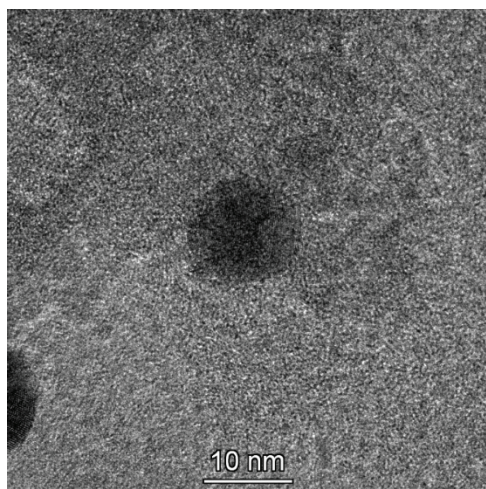


Figure 1: TEM image of one BiSb nanoparticle.

1. Tang, S. and M.S. Dresselhaus, *Electronic properties of nano-structured bismuth-antimony materials*. Journal of Materials Chemistry C, 2014. 2(24): p. 4710-4726.

OPTIMIZING SiC INTERLAYERS FOR THERMAL MANAGEMENT IN DIAMOND/ β -Ga₂O₃ HETEROJUNCTION DEVICES.

Pujan Lamsal², Pallab Sarkar¹, and Ariful Haque^{1,2},
¹Materials Science, Engineering, and Commercialization (MSEC), and ²Electrical Engineering, Ingram School of Engineering, Texas State University, San Marcos, TX 78666, USA.

Beta Gallium Oxide (β -Ga₂O₃) has gained significant attention in the field of high-power electronics due to its ultra-wide bandgap and excellent electronic properties, enabling high breakdown voltage and energy-efficient operation. However, its inherently low thermal conductivity (~ 27 W/m·K) creates challenges for heat dissipation, leading to performance limitations and reduced reliability under high-power operation. To address these thermal management issues, this study explores the incorporation of Silicon Carbide (SiC) as a buffer layer and diamond as a heat spreader in β -Ga₂O₃. The SiC interfacial layer is particularly advantageous compared to conventional interfacial materials like SiO₂ or Si₃N₄, which are typically used for Si, GaN or Ga₂O₃ industry. Recent findings show that during diamond deposition, carbon particles can break down SiO₂ at the interface to form SiC, indicating SiC's natural compatibility in such heterojunction devices. Moreover, studies have recorded significantly lower thermal boundary resistance (TBR) at SiC interfaces in Diamond/GaN and Diamond/Si integrations, further motivating its direct use as an interfacial material for improved thermal management in Ga₂O₃/Diamond based devices. The fabrication process involves depositing β -Ga₂O₃ films via Pulsed Laser Deposition (PLD), followed by RF sputtering of thin SiC interlayer, and diamond deposition using Hot Filament Chemical Vapor Deposition (HFCVD). The SiC interfacial layer serves two critical roles in β -Ga₂O₃-based devices. Its low lattice mismatch ($\sim 1.3\%$) and closely matched coefficient of thermal expansion (CTE) minimize interfacial strain and thermal stress, enabling stable and efficient thermal transport. Additionally, SiC acts as a protective barrier during diamond deposition via HFCVD, shielding the β -Ga₂O₃ substrate from degradation caused by reactive H₂ radicals and the harsh deposition environment. This work aims to optimize the SiC layer thickness to protect the Ga₂O₃ substrate during the HFCVD process, minimizing TBR, enhancing phonon transfer, and ensuring efficient thermal management through a smoother Ga₂O₃/diamond interface. Cross-sectional Secondary Electron Microscopy (SEM) images in Fig. 1 reveal that a 45 nm SiC interlayer effectively protects the Ga₂O₃ layer from etching or decomposition during the diamond deposition process, while enabling the formation of a smooth and well-defined interface between the Ga₂O₃ film and a 208 nm-thick diamond layer grown over 30 minutes, providing a basis for further

investigation into the thermal transport characteristics of these structures. These findings pave the way for more efficient and reliable high-power electronic devices, unlocking the full potential of β -Ga₂O₃ for advanced thermal management solutions.

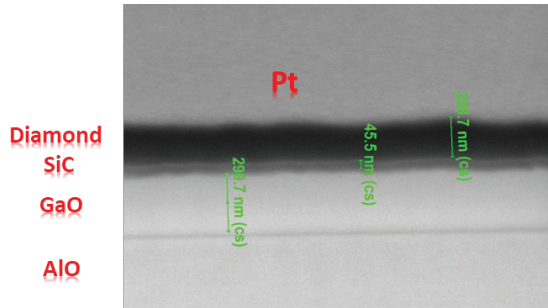


Fig. 1 – Cross sectional view between Diamond and β -Ga₂O₃ heterojunction with thin SiC interfacial layer

MINERALOGICAL AND TEXTURAL ANALYSIS OF COSMIC DUST COLLECTED DURING THE 2012 DRACONID METEOR SHOWER

Alan E. Martinez^{1,2}, Prajkta Mane¹, and Lindsay P. Keller³.
¹Lunar and Planetary Institute, USRA, 3600 Bay Area Blvd, Houston, TX 77058. ²Texas State University, 601 University Dr, San Marcos, TX 78666. ³NASA Johnson Space Center, Mail Code XI3, Houston, TX 77058.

Introduction: Interplanetary Dust Particles (IDPs) are small (~ 5-50 μ m), complex assemblages of crystalline and amorphous phases found within the interplanetary medium. Chondritic porous IDPs (or CP-IDPs) have fluffy and porous textures along with an anhydrous silicate mineralogy and are thought to have originated from comets [1]. We aim to study the mineralogy and textural characteristics of a CP-IDP collected by the NASA Cosmic Dust collection to understand the origins and secondary processes that are recorded within the dust particle. While the IDP selected for this work is from a targeted collection, the specific cometary origin of an individual IDP is difficult to establish unambiguously as some IDPs from targeted collections may be from a non-specific source [2]. However, Keller et al., 2021 [3] showed that as IDPs travel within the interplanetary medium, they are bombarded by solar energetic particles (SEPs) leaving defects called solar tracks that can be studied to determine the exposure age of the IDPs by assessing the track density recorded in the crystalline silicates. IDPs from the parent-body of the Draconid meteor shower, 21P/Giacobini-Zinner, have short exposure times and are not expected to show either SEP tracks or high abundances of implanted solar wind gases [4].

Methods: We were allocated CP-IDPs retrieved from flag U2153 flown on the NASA high altitude ER-2 aircraft during the 2012 Draconid meteor shower. We prepared particle U2153-S1 for Transmission Electron Microscopy (TEM) analysis by mounting it in Embed-812 epoxy using

a clean glass needle. The epoxy was cured for 48 hours at 70 °C and thin sections (\approx 70 nm thick) of the particle were prepared and collected on an amorphous carbon-coated Cu TEM grid using a Leica EM UC6 Ultramicrotome. These sections were analyzed using the JEOL 2500 SE 200keV Scanning Transmission Electron Microscope (S) TEM at NASA Johnson Space Center. Both Bright Field (BF) and Dark Field (DF) micrographs were taken to search for solar tracks and determine the textures and mineralogy of the particle. Additionally, the JEOL thin window Energy Dispersive X-ray (EDX) spectrometer was used to map the composition of the mineral grains.

Results: TEM analysis of the IDP U2153-S1 shows a porous texture shown in Fig 1a. along with anhydrous crystalline silicates like enstatite (Fig. 1c) and olivine (Fig. 1e) which typically preserve solar tracks. The twin planes found along the enstatite grain indicate the mineral formed at high temperatures (\sim 1200 and 1300°C) [1]. This CP-IDP also contains polycrystalline aggregates called Glass Embedded with Metal Sulfides (GEMS) shown in Fig. 2a which are rich in both silicates and carbonaceous materials. Notably, the magnetite (Fe₃O₄) partial rim structure found on the GEMS cluster indicates heating during atmospheric entry and the presence of nitrogen (Fig. 2d) could suggest cometary volatiles were preserved in the GEMS assemblage. Another distinct structure found within the IDP are Equilibrated Aggregates (EAs) which have been found to be assemblages of iron-bearing olivines and pyroxenes with equilibrated ratios of Fe/Mg and iron sulfides within aluminosilicate glass [1]. The presence of a triple junction in Fig. 1g is a common feature of annealing in EAs which can suggest heating in early-sun conditions or by nebular shocks during the early solar system [5].

Discussion: Based on the mineralogy seen in the TEM micrographs, EDX spectra, and textures we can determine this IDP is likely to be of cometary origin and draw connections to its targeted parent body, 21/P Giacobini-Zinner. Studies of the comet using Mid-Infrared Spectroscopy [6] suggest the comet is rich in organic molecules, supported by the high abundance of carbon (Fig. 2c.) in addition to the observed silicate grains olivine and pyroxene (enstatite) (Fig. 2d). The solar track calibration used in Keller et. al (2021) [3] was applied to the observed silicate minerals olivine and enstatite and shown to have an area of 84 and 48 μ m², respectively. For observable tracks to form in these grains would mean the particle would have had to be in the interplanetary medium for \sim 3000 years or more from deposition to collection. While solar tracks can be erased by high thermal processes (\approx 500-600°C) during atmospheric entry [1], melting of the silicates and sulfides within the particle was not observed, so it is unknown if the high Earth encounter velocity which formed the partial magnetite rim shown in Fig. 2 caused the particle to reach the necessary temperatures to erase preserved solar

tracks. As this study only reports the properties of a single IDP, future work will focus on understanding the diversity of mineralogical and textural properties of IDPs found in other targeted collections such as the Pi Puppids and Perseids meteor shower. These studies will provide further evidence to understand the diversity of cometary material that is recorded within these targeted interplanetary dust particles.

References: [1] Bradley, JP (2014) *Treatise on Geochemistry (Second Edition)* 287-308. [2] Davidson, J. et al. *Meteoritics & Planet. Sci.*, 47, 1748-1771. [3] Keller, L.P. et. al (2021) *Meteoritics & Planet. Sci.*, 56, 1685-1707. [4] Messenger, S. (2002) *Meteoritics & Planet. Sci.*, 37, 1491-1505 [5] Keller, L.P., et. al (2009) LPSC XL, Abstract #2121. [6] Ootsubo et al. (2020) *Icarus* 338 113450.

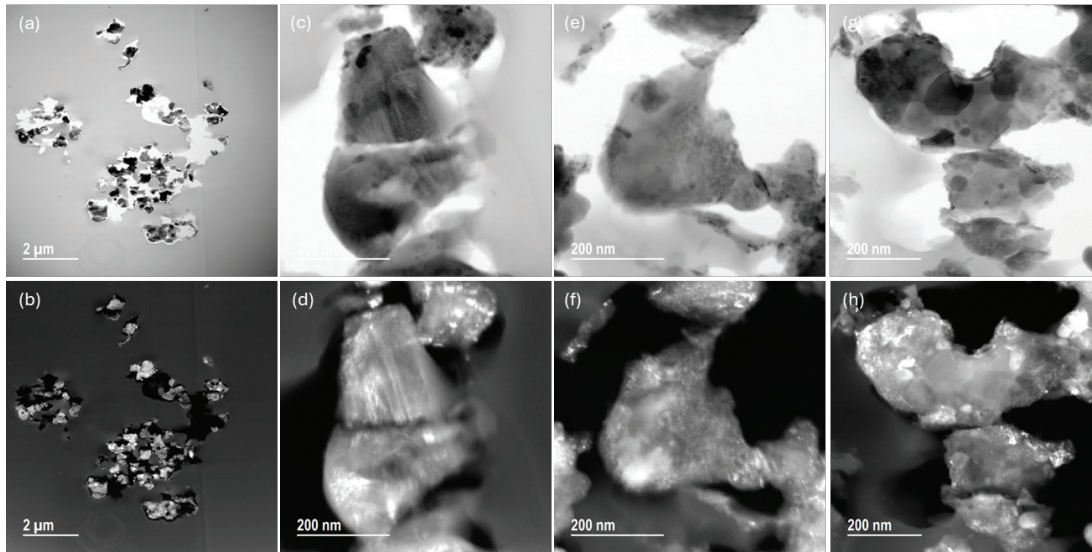


Figure 1. (a) BF-TEM image of section of U2153 showing CP-IDP structure. (b) DF-TEM image showing the crystalline material within the IDP cross section. (c) BF-TEM image of enstatite grain (d) DF-TEM image showing prevalent enstatite twinning and no evidence of solar tracks. (e) BF-TEM image of olivine grain (f) DF-TEM image of olivine showing no evidence of solar tracks. (g) BF-TEM image of an Equilibrated Assemblage (EA) showing prevalent triple junction. (h) DF-TEM image of an EA showing its crystallinity.

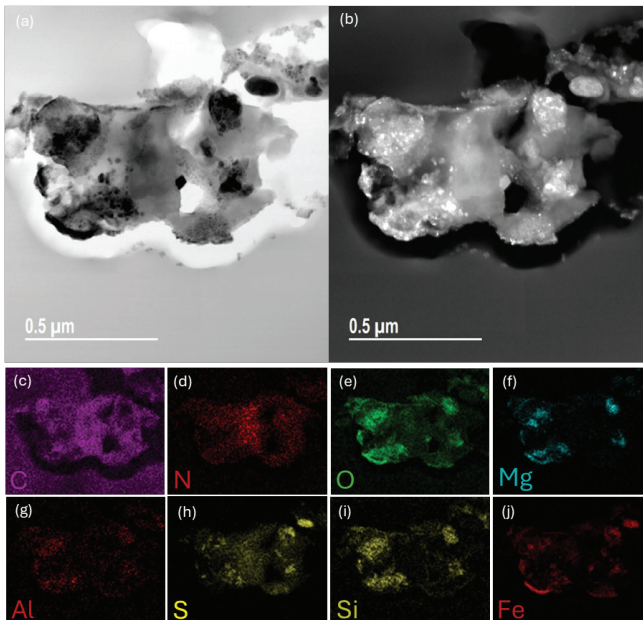


Figure 2. (a) BF-TEM image of GEMS cluster (b) DF-TEM showing crystalline GEMS material (c) EDS map of Carbon (d) EDS map of Nitrogen (e) EDS map of Oxygen (f) EDS map of Magnesium (g) EDS map of Aluminum (h) EDS map of Sulfur (i) EDS map of Silicon (j) EDS map of Iron.

Acknowledgments: This work was supported by the Lunar and Planetary Institute's (LPI's) 2024 Summer Intern Program in Planetary Science and a Cooperative Agreement Expanding NASA's Community of Planetary Sample Scientists (ENComPSS) between NASA's Science Mission Directorate and the LPI, which is operated by the Universities Space Research Association (USRA).

ADVANCING ENERGY RESEARCH IN ENERGY PRODUCTION & STORAGE USING *IN SITU* LIQUID-PHASE TEM

Gabriela Mendoza, Dylan Wood, Jennifer McConnell, and Madeline Dukes

Protochips, Inc, Morrisville, NC 27560, USA

In situ transmission electron microscopy (TEM) can reveal the dynamic mysteries of materials at the level of their origin: the nanoscale. Material properties and operational performance are completely dependent upon a material's behavior at the nanoscale; however, on any given day, we typically only see macroscale behavior, which is simply an aggregation of millions of nanoscale processes occurring simultaneously.

In-situ TEM is commonly used to study clean fuel production, energy production & storage, and materials design. This presentation will demonstrate the application of a cooling liquid cell *in-situ* TEM holder (Triton AX, Protochips Inc.) for the characterization of robust and cost-efficient materials for lithium-ion batteries, solid-state batteries, and hydrogen fuel-cells (Figure 1). The holder can simultaneously control temperature and electrochemistry, enabling observation of nanoscale dynamic behavior under relevant operating conditions, such as a wide range of organic and aqueous liquid media, a miniaturized electrochemical cell with standard electrode materials, and an ultra-sensitive electrochemical framework, all within the TEM (Figure 1). An overview of the most recent applications utilizing the *in-situ* holder and a machine vision *in situ* workflow will be provided.

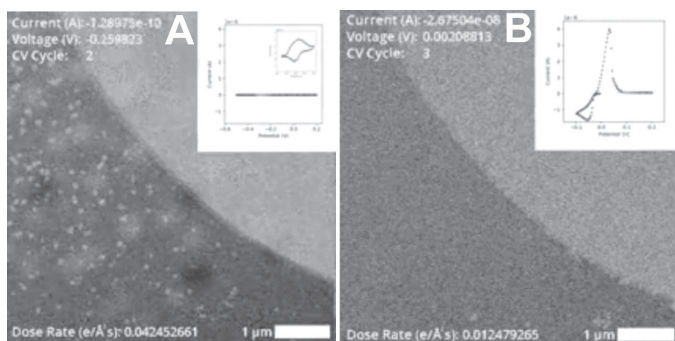


Figure 1: *In-situ* STEM micrographs of copper sulfate electrolyte (50mM) in sulfuric acid (0.1M) flowing at 10 $\mu\text{l/h}$. STEM micrograph and cyclic voltammetric curve of Pt working electrode with copper plating layer at 5°C (A) and 98°C (B). Dendrite morphology, kinetics, and current measurements differ significantly at (A) 5°C (smaller, slower, and lower, respectively) from those at (B) 98°C. The insets show the CV curve with smaller y-axis, demonstrating that even without visual changes, there is still a reaction occurring, even though the near-freezing temperature has slowed the reaction down significantly.

USE OF SCANNING ELECTRON MICROSCOPY IN MORPHOLOGICAL STUDY OF SOLUTION-PROCESSABLE MOF-GRAPHENE NANOCOMPOSITE FOR ORGANIC SOLAR CELL APPLICATIONS

Nhan Pham, Md Abdul Halim, Ariful Haque

Department of Electrical Engineering, Ingram School of Engineering, Texas State University, San Marcos, TX 78666 USA

This research focuses on addressing the limitations of traditional high-cost, high-temperature semiconductor thin film deposition techniques by developing a solution-processable inkjet printing method for organic solar cells (OSCs). Specifically, we propose using exfoliated two-dimensional (2D) metal-organic frameworks (MOFs) combined with graphene nanocomposites to create a cost-effective and efficient photoactive layer. Tetracyanonickelate (TCN) based MOFs, which exhibit intrinsic porosity and alterable optoelectronic properties, are exfoliated using liquid phase exfoliation (LPE) to form otherwise low conductivity ultrathin nanosheets. The conductivity of nanosheets can be improved by adding commercially available carbon-based materials such as graphene or reduced graphene oxide (rGO), thus forming a nanocomposite. Scanning Electron Microscopy (SEM) reveals the exfoliated 2D morphology of the nanosheets which is key to obtaining the highly active surface area. The SEM image in Figure 1 shows the typical morphology of the material. Nanosheets group into particles with an average particle size of 500nm can be exfoliated into nanosheet of 20nm-200nm thickness. The specific surface area calculated for these materials is graphite. X-ray diffraction and Raman spectroscopy confirmed the presence of carbon triple bond and carbon nitrogen bond, no impurities were observed in 5 trials. A nanocomposite bandgap was measured using a four-point probe and UV-Vis Spectrophotometry. This approach offers a scalable, flexible, and low-cost deposition method for organic solar cells (OSCs), with the potential for improved performance and mass customization through inkjet printing. The study aims to overcome current challenges in improving conductivity while leveraging the processability and flexibility of solution processable MOFs in organic solar cells.

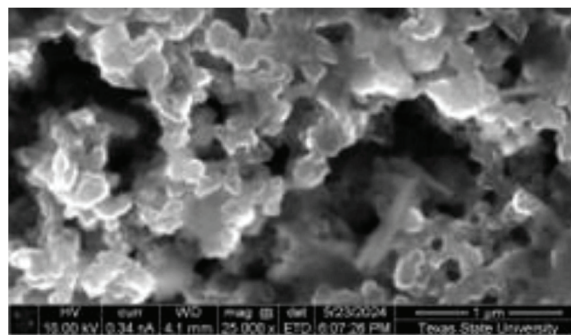


Figure 1: SEM image of Exfoliated Nanosheet Morphologies of TCN MOF-Graphene Nanocomposite.

STRUCTURE-PROPERTY AND STRUCTURE-BEHAVIOR RELATIONSHIPS OF CARBON NANOTUBES SUBJECT TO IMPACT INDUCED MORPHOLOGY CHANGE

Mason Rhue, Brian Grady

School of Sustainable Chemical Biological and Materials Engineering, University of Oklahoma, Norman, OK 73019

Carbon nanotubes are promising alternatives to other carbon-based fillers for polymer composites due to their outstanding mechanical, electrical, thermal, and morphological properties. However, their widespread application in electronics and aerospace industries is limited by low synthesis yields and the need for purification. Our group has recently developed a high yield synthesis process capable of growing very long carbon nanotubes on multilayered catalyst supports (Figure 1). The total carbon yield (>95 wt%) is the highest yet reported for scalable nanotube synthesis processes, and the need for purification is eliminated due to the product purity. The carbon nanotubes produced in this process are approximately 100 μm in length and 15 nm in diameter ($L/D > 6,000$) and are among the highest aspect ratio nanotubes previously studied in the context of polymer nanocomposites. While the implications of ultrahigh aspect ratio carbon nanotubes are largely positive (e.g., low loadings required for good mechanical and electrical reinforcement in composites), high aspect ratio fillers have been shown to result in high composite melt viscosities, leading to polymer degradation and reduced composite properties. Thus, we employ ball milling as a simple, inexpensive, scalable process for reducing carbon nanotube length prior to compounding in polymers. In this work, we discuss the various basic microscopy techniques that inform structure-property and structure-behavior relationships of carbon nanotubes subject to these impact induced morphology changes.

Using scanning electron microscopy (SEM), the bulk morphology of carbon nanotubes can be examined. We found that most commercial carbon nanotubes are supplied in the form of randomly agglomerated bundles on the order of 1 μm in diameter, whereas the ultrahigh aspect ratio nanotubes produced in our process are almost exclusively aligned in larger bundles on the order of 10 μm in diameter. Additionally, accurate length measurement of carbon nanotube bundles and individual carbon nanotubes can be achieved using SEM along with image stitching/processing software, allowing for the establishment of a correlation between input ball milling energy and the resulting length reduction of a milled carbon nanotube sample. We can also examine the individual wall morphology of carbon nanotubes using high resolution transmission electron microscopy (HR/TEM). We found that for most commercial parallel walled carbon nanotubes (Figure 2 - left), the minimum single impact energy input required for nanotube fracture scaled linearly with nanotube diameter (Figure 3). However, for a nanotube sample with prevalent cup stacked wall morphologies (Figure 2 - right), the minimum single impact energy input required for nanotube fracture is significantly reduced due to the weaker van der Waals forces holding the nanotube together compared to parallel walled morphologies. Additionally, we found that the bulk morphology, particularly bundle alignment and diameter, plays a large role in determining the minimum energy input for fracturing any nanotube inside a bundle. By systematically varying ball mill input energy and accurately measuring carbon nanotube lengths by SEM, we were able to develop a milling energy master curve (Figure 4) that can accurately predict the length reduction kinetics of any milled carbon nanotube sample if the initial length is known, regardless of the wall morphology. While the microscopic techniques used here are basic, the structure-property and structure-behavior relationships elucidated were critical to the basis of this work.

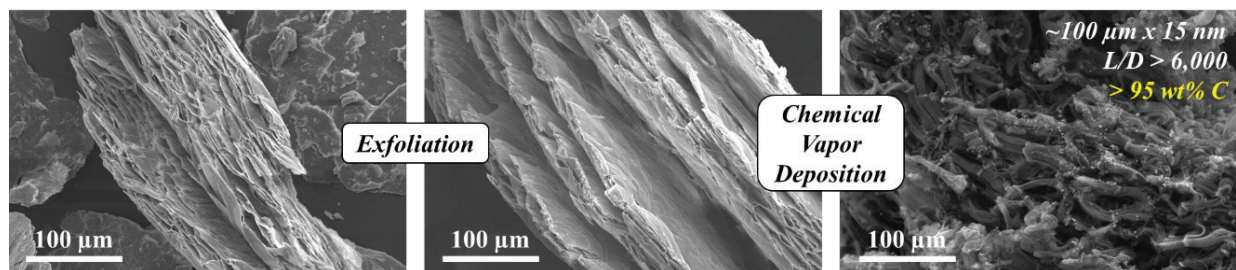


Figure 1. Ultrahigh aspect ratio carbon nanotubes synthesized on exfoliated vermiculite support.

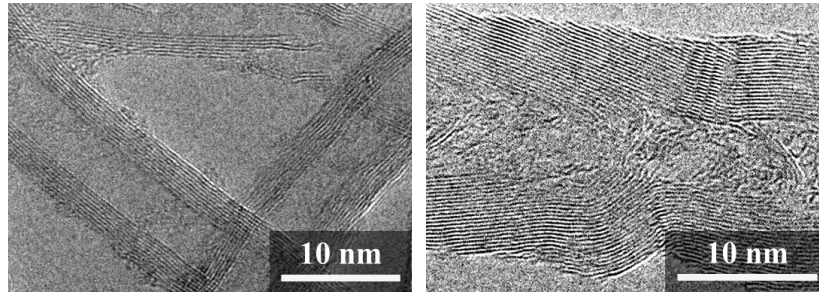


Figure 2. Parallel walled (left) and cup stacked (right) carbon nanotube wall morphologies.

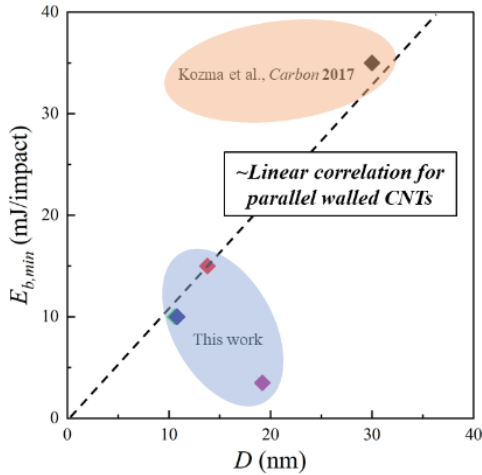


Figure 3. Minimum single impact energy dependence on carbon nanotube diameter for a variety of commercially available carbon nanotubes.

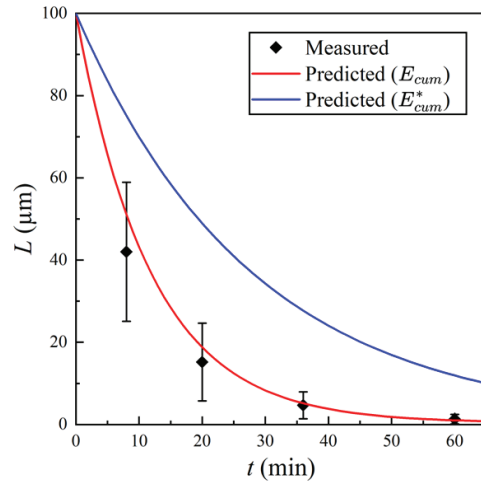


Figure 4. Extrapolating the length reduction behavior of short (~1 μm length), commercial carbon nanotubes accurately predicts the length reduction of ultrahigh aspect ratio (~100 μm length) carbon nanotubes.

NON-DESTRUCTIVE CHARACTERIZATION OF BATTERIES AND BATTERY MATERIALS USING X-RAY COMPUTED TOMOGRAPHY.

Angela Criswell, Tai-Jan Haung, Department of X-ray Imaging, Rigaku Americas Corporation, The Woodlands, TX 77381.

Non-destructive characterization techniques are essential for the development and performance evaluation of batteries and battery materials. X-ray computed tomography (CT) has emerged as one of these powerful techniques because it provides information about the internal structure of batteries without the need for teardown. Additionally, X-ray CT allows imaging across multiple length scales, making it a valuable tool to characterize battery materials at high resolution and inspect battery cells and packs. Additionally, X-ray CT allows researchers to characterize degradation and failure mechanisms with charge/discharge cycles, revealing phenomena such as electrode cracking, delamination, and dendrite formation. The ability to conduct non-destructive analysis at multiple length scales – from micro to nano – makes X-ray CT a versatile technique for optimizing battery design, improving performance, and investigating failure mechanisms. In this study, we show how X-ray CT is applied to inspect batteries and battery material and extract

quantitative data that provides meaningful insights into their structure and function.

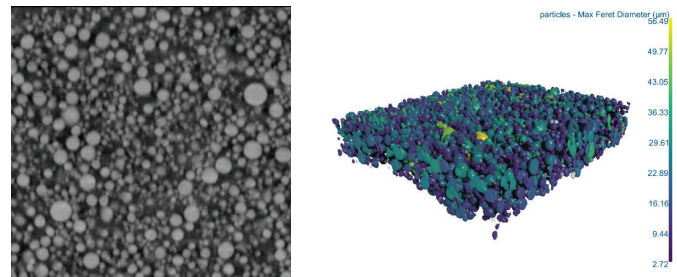


Fig.1 X-ray CT inspection of cathode material and quantitative analysis of cathode particle size.

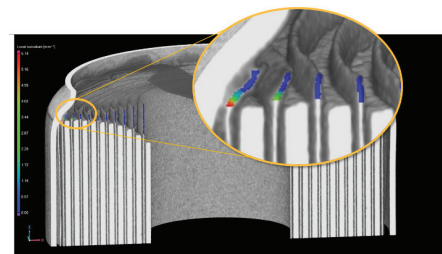


Fig.2 Battery cell inspection and overhang analysis for an 18650 cylindrical cell.

X-RAY COMPUTED TOMOGRAPHY FOR NON-DESTRUCTIVE 3D STRUCTURAL CHARACTERIZATION IN ADDITIVE MANUFACTURING.

Tai-Jan Haung, Angela Criswell, Department of X-ray Imaging, Rigaku Americas Corporation, The Woodlands, TX

Additive manufacturing (AM) offers significant geometric flexibility for novel structure fabrication and a combination of diverse material options that are challenging or unattainable using traditional manufacturing methods. However, these capabilities also introduce increased structural complexity and associated challenges. Advanced characterization techniques are hence essential to obtaining detailed insights into the resulting structures and processing outcomes through AM.

X-ray computed tomography (CT) is a non-destructive characterization method that provides three-dimensional structural data without stringent dimensional constraints or extensive sample preparation. Its ability to capture high-resolution, inherently 3D datasets facilitate a comprehensive understanding of structural properties without sampling bias. Furthermore, X-ray CT enables the transition of correlation studies from two-dimensional analysis to three-dimensional space and is highly compatible with both ex-situ and in-situ scenarios.

This work demonstrates the use of X-ray CT for structural characterization in various types and stages of additive manufacturing, including the quantification and spatial distribution of defects, analysis of microstructure evolution, and mechanical load simulations.

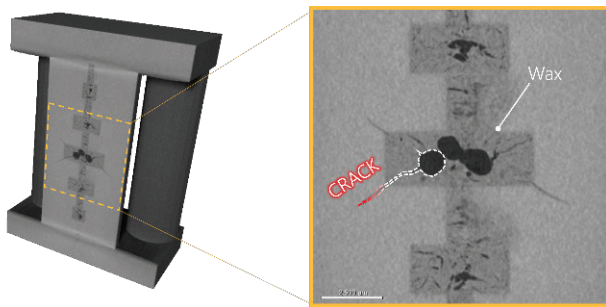


Fig.1 Photopolymer

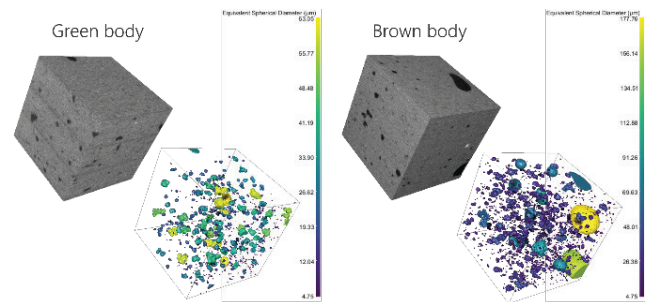


Fig.2 Laminated ceramic

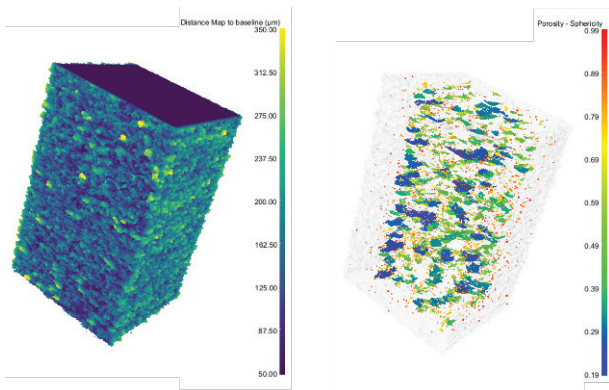


Fig.3 Powder bed fusion Titanium alloy

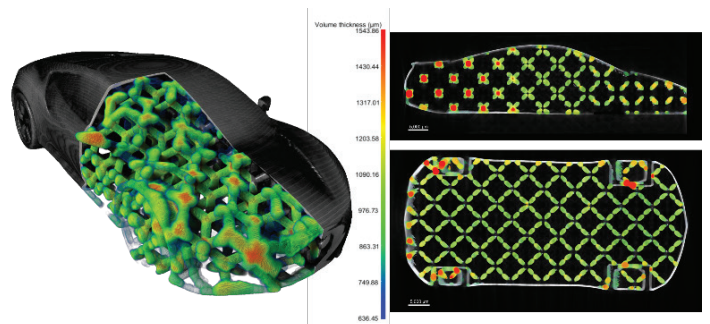


Fig.4 Inconel® superalloy

AN EDUCATION PROGRAM TO ASSIST MID-CAREER PROFESSIONALS TO TRANSFER TO A MICROSCOPY CAREER.

Keith Holcomb, Mark Armitage, DSTRI.org, Sequim, WA, 98382.

Mid to late career professionals (particularly prospective retirees) experience steep challenges when faced with the desire to switch careers entirely and seek a challenging working adventure far removed from their own experience [1, 2, 3, 4]. This can be especially challenging when transferring from a non-academic, non bench-top-science career (aviation for example), into a hard-science opportunity like microscopy. A wide variety of career choices exist within the field of microscopy (a fact not readily apparent to an aviator), however without adequate motivation, proper training and mentorship/education, employment opportunities such as 'light microscopist' are simply unavailable to professionals who might consider it a possibility. There is certainly no substitute for training and education in any science. Often decades of study are undertaken to excel at science. Thankfully regional programs of study are available within travel distance for those who can afford it. But might the prospect of all that daunting training deflate the prospective second career professional? Motivation might seem a trivial matter to consider when navigating the winding trail of starting again at 60. But in the first author's case, motivation was everything and it came from a microscopist who had amazing paleontological specimens and was searching for students. In this presentation we briefly review the implementation of planning, education and execution modalities that have allowed the first author to transition from an advanced status aviation career (40+ years) into a microscopy-based science career (including rewarding microscopy/publication and presentation opportunities). Modalities include acquiring professional-grade instruments, conducting guided research on fresh paleontological specimens, mastering dissecting and compound microscopy, photomicrography (Figures 1,2), specimen processing and polarised light under guided mentoring. All these can lead one to microscopy that clearly advances science as shown. With involvement in local area microscopy societies, attendance and participation at other microscopy meetings (like M&M), along with volunteering in labs, the first author has been led to begin mentoring young students to do likewise. Now giving back to our youth is an unexpected reward.

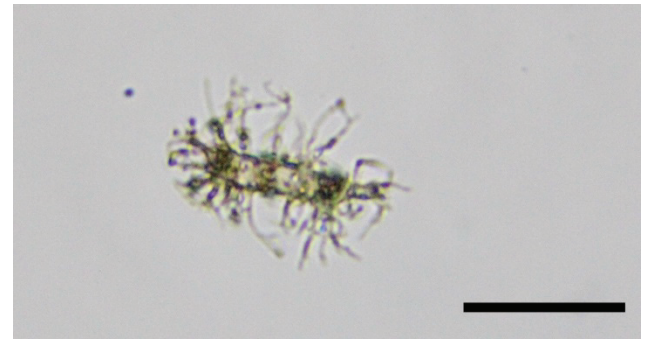


Figure 1 Brightfield (BF) Osteocyte, demineralized surface shard Scale bar = 18 μ m



Figure 2 Brightfield (BF) Osteocyte matrix, demineralized surface shard. Scale bar = 25 μ m

References:

1. Nalis I, Kubicek B and Korunka C (2021) From Shock to Shift–A Qualitative Analysis of Accounts in Mid-Career About Changes in the Career Path. *Front. Psychol.* 12:641248. doi: 10.3389/fpsyg.2021.641248
2. Ruiz Castro, M., Van der Heijden, B.I.J.M. & Henderson, E.L. (2020). Catalysts in career transitions: Academic researchers transitioning into sustainable careers in data science. *Journal of Vocational Behavior.* <https://doi.org/10.1016/j.jvb.2020.103479>.
3. Haasler, S., & Barabasch, A. (2015). The role of learning and career guidance for managing mid-career transitions - comparing Germany and Denmark. *British Journal of Guidance & Counselling*, 43(3), 306-322. <https://doi.org/10.1080/03069885.2015.1020758>
4. Mid-Career Professionals in STEM Transiting to School Teaching: Barriers at the Border. James J Watters and Carmel M Diezmann Queensland University of Technology, Brisbane j.watters@qut.edu.au 2nd International STEM in Education Conference

Au-flat™

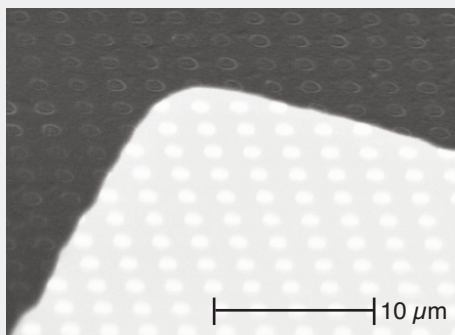
**Electron
Microscopy
Sciences**

Gold Foil Sample Supports for Cryo-EM

FOR HIGH RESOLUTION IMAGING

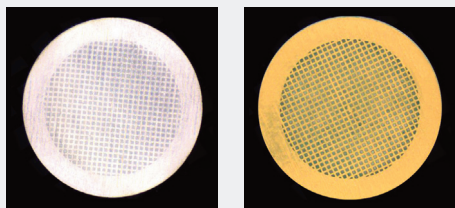
Au-flat™ is an ultrastable Cryo-EM sample support with a 45nm holey Gold alloy film on 3mm gold mesh grids. Au-Flat is a derivative of our patented C-flat™ product.

UNIFORM VITREOUS ICE ACROSS THE GRID



Au-flat uses new, ultra-flat precision gold grids which create a more planar surface. The result is **more uniform thin ice** across the entire surface, including areas near the grid bars.

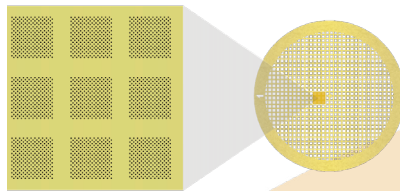
NO MISTAKES



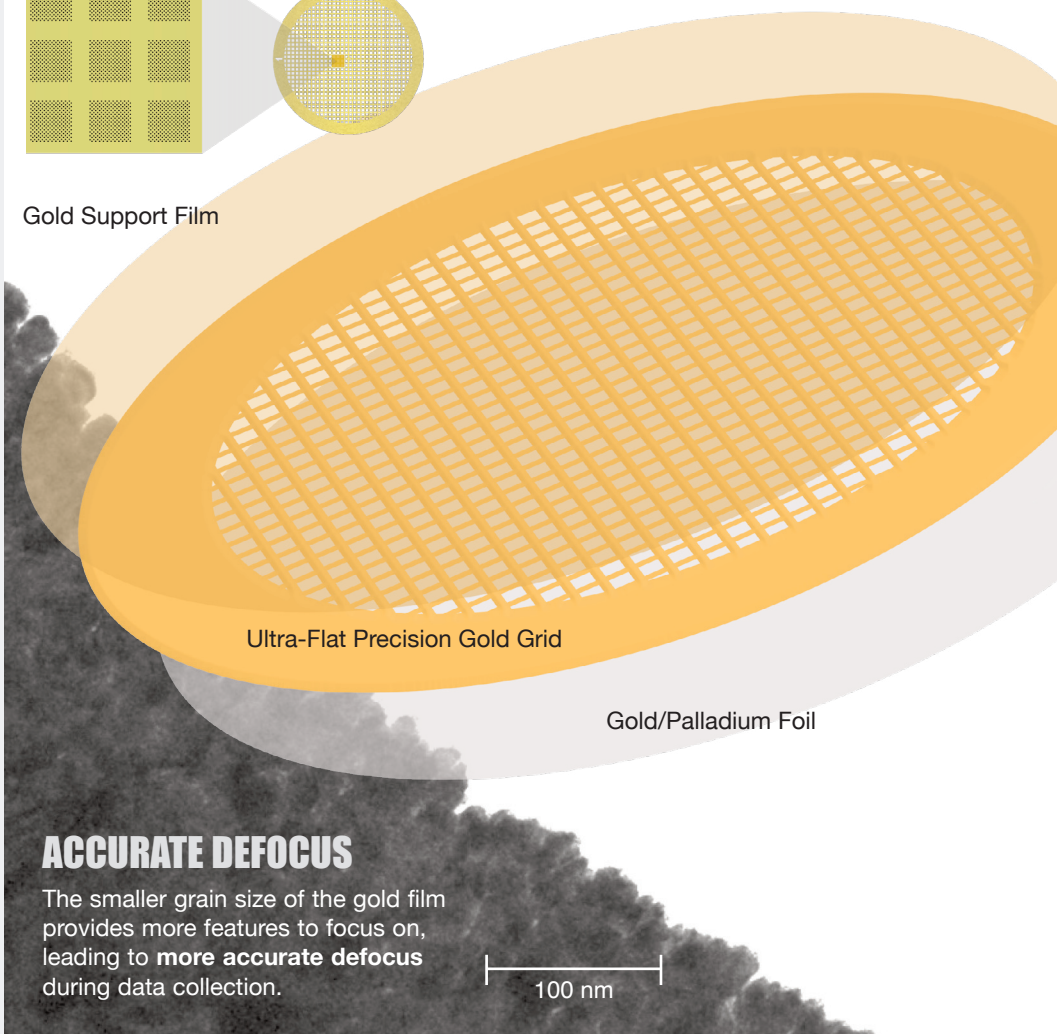
Au/Pd Foil Side

Gold Mesh Side

The lighter color of the Au-Pd film compared to the underlying gold mesh grid makes it **easy to identify** the film side of the grid during sample preparation.



Gold Support Film



Ultra-Flat Precision Gold Grid

Gold/Palladium Foil

ACCURATE DEFOCUS

The smaller grain size of the gold film provides more features to focus on, leading to **more accurate defocus** during data collection.

WHAT ARE THE BENEFITS OF AU-FLAT OVER HOLEY CARBON SUPPORTS?

Better reconstructions with less data

Au-flat significantly reduces beam-induced motion during imaging compared to carbon films, improving image quality and resolution.

Biocompatible

Au-flat features a holey Au/Pd film on a gold mesh grid, so it's chemically inert and biologically compatible.

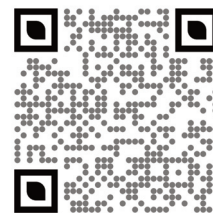
Durable

Au-flat's film is significantly stronger than carbon films and is more capable of surviving the Cryo-EM workflow including tweezer handling, glow discharge, blotting, auto-grid loading and plunge freezing.

Stronger

Au-flat is produced with gold mesh grids that are about 6μ thicker than typical Cryo-EM grids. This makes the grids stiffer and less likely to bend or deform. The increased thickness is fully compatible with side-entry holders as well as auto-loaders.

Find out more
about **Au-flat™**



**Electron
Microscopy
Sciences**

POWERED BY BIOLYST

1560 Industry Rd.
Hatfield, Pa 19440
email: info@emsdiasum.com
www.emsdiasum.com

Corporate Members and Regional Sales Managers



3i Intelligent Imaging Innovations

intelligent-imaging.com
3575 Ringsby Ct, Suite 102
Denver, CO 80216, USA
Tel: 303-607-9429
Daniel Giardina
daniel.giardina@intelligent-imaging.com
Jason Jacoby
jason.jacoby@intelligent-imaging.com



Advanced Microscopy Techniques

amtimaging.com
242 West Cummings Park
Woburn, MA 01801
Dominick Camillo
508-221-4449; dominick@amtimaging.com
Tom Levesque
214-883-3194; tlevesque@amtimaging.com
Adam Maganiello
508-221-4449; adam@amtimaging.com



AMETEK, GATAN, EDAX

ametec.com
780 Commonwealth Dr
Warrendale, PA 15086
Phone: 201-529-4880
John Haritos
512-745-5954; John.haritos@ametec.com
Stephen Mick
Stephen.mick@ametec.com
David Stowe
David.Stowe@ametec.com



Andor Instruments, an Oxford Company

andor.oxinst.com/
860 Aviation Pkwy Ste 1400
Morrisville, NC 27560
Phone: 408-850-1139
Tomas Silva Santisteban
tomas.silva@oxinst.com
Ryan Robinson
ryan.robinson@oxinst.com



AVR Optics

avr-optics.com
187 N Water Street
Rochester, NY 14604
Lane Manning
585-445-7588; lane.manning@avr-optics.com



Improve Research Reproducibility

Bio-protocol LLC

bio-protocol.org/
1075 Lorne Way
Sunnyvale, CA 94087, USA
Fanglian He
fhe@ed.bio-protocol.org



BioTek is
now Agilent!

BioTek Instruments, Inc. (Now Agilent)

biotek.com
5301 Stevens Creek Blvd.
Santa Clara, CA 95051
David Kurtz
847-757-3387; kurtzd@biotek.com



Boeckler Instruments, Inc.

boeckler.com
4650 S. Butterfield Drive
Tucson, AZ 85714
Phone: 520-745-0001
Fax: 520-745-0004
Peter Strucks
520-331-2216; peter.strucks@boeckler.com



Bruker AXS, Inc.

bruker.com
3194 Beverly Court
Murrysville, PA 15668
Phone: 908-419-8225
Austin, TX 78747
Jeffrey Hannon
608-867-7680; Jeffrey.Hannon@bruker.com
Stephen Ziegler
737-262-5004; Stephen.Ziegler@bruker.com



Cameca Instruments, Inc.

cameca.com
5470 Nobel Drive
Phone: 608-274-6880
Madison, WI 53711
Steve Foldvari
608-229-1486; steve.foldvari@ametec.com
Dan Jacobson
831-241-2845; dan.jacobson@ametec.com



A BICO COMPANY

Discover Echo Inc.

discover-echo.com/
9530 Padgett St., Suite 101
San Diego, CA 92126
Adam Conway
617-999-2774;
aconway@discover-echo.com
Joanna Harper
617-999-2774; jharper@discover-echo.com
Brian Templin
713-557-8915; btemplin@discover-echo.com

Electron Microscopy Sciences

Electron Microscopy Science

emsdiasum.com/microscopy/
1560 Industry Road, P.O. BOX 550
Hatfield, PA 19440
Phone: 800-523-5874
Fax: 215-412-8450
Stacie Kirsch
215-415-8400; skirsch@biolyst.com
Robert Armstrong
215-412-8400; kmc michael@biolyst.com



EVIDENT SCIENTIFIC

(formerly Olympus Scientific Solutions
Americas)
EvidentScientific.com
48 Woerd Avenue
Waltham, MA 02453 USA
Phone: 1-800-225-8330
Eric Bridenbaugh (Life Science)
Phone: 512-800-9332
Eric.Bridenbaugh@evidentscientific.com
Joseph Lake (Material Science)
Phone: 469-580-7565
Joseph.lake@evidentscientific.com



E.A. Fischione Instruments, Inc.

fischione.com
9003 Corporate Circle
Export, PA 15632
Phone: 724-325-5444
Nicole Dengler
724-325-5444; nm_dengler@fischione.com
Paulina Koszowska
724-325-5444; p_koszowska@Fischione.com

Hirox USA, Inc.

hirox-usa.com
100 Commerce Way
Hackensack, NJ 07601
Phone: 201-342-2600
Edvina Bassano
201-342-2600; edvina@hirox-usa.com
Cody Driver
201-342-2600; driver@hirox-usa.com

Inspire the Next**Hitachi High Technologies America**

hitachi-hta.com
1375 North 28th Ave.
PO Box 612208
Irving TX 75261
Phone: 214-537-2158
Fax: 972-615-9300
Robert Passeri - 847-946-3788;
robert.passeri@hitachi-hightech.com
Matthew Reinoehl - 847-946-3788;
matthew.reinoehl@hitachi-hightech.com

Horiba Scientific

horiba.com/int/scientific/
20 Knightsbride Rd.
Piscataway, NJ 08854
Chris John
415-996-3510; chris.john@horiba.com
Andrey Krayev
415-996-3510; andrey.krayev@horiba.com

**IXRF Systems**

ixrfsystems.com
10421 Old Manchaca Rd., Suite 620
Austin, TX 78748
Phone: 512-386-6100
Fax: 512-386-6105
Bryan De Verse
512-386-6100; bryand@ixrfsystems.com
Andrea Surak
andreas@ixrfsystems.com
Robert Tisdale
512-415-6839; robertt@ixrfsystems.com

Solutions for Innovation

JEOL USA, Inc.

http://www.jeolusa.com
13810 Paisano Circle
Austin, TX 78737
Phone: 978-495-2176
Joel Paul
978-979-8071; jpaul@jeol.com
Carolyn Rogers
978-536-2308; crogers@jeol.com
Noureddine Anibou
978-998-2726; nanibou@jeol.com

Kleindiek Nanotechnology

Kleindiek.us
3526 3rd St N, Arlington VA 22201
Phone: 925-400-8306
Lorenz Lechner
925-400-8306; lorenz.lechner@kleindiek.us
Kevin Kaime
kevin.kaime@kleindiek.us

MICROSYSTEMS

Leica Microsystems, Inc.

http://www.leica-microsystems.com
7125 Northland Terrace N., Suite 100
Brooklyn Park, MN 55428
Phone: 314-374-9361
Andrew Lawson - 469-785-9992;
Andrew.Lawson@leica-microsystems.com

Lifecanvas Technologies

lifecanvastech.com
1035 Cambridge Street Ste. 16C,
Cambridge, MA 02141
Ali Balaguer
628-268-5113; ali@lifecanvastech.com

Lumencor, Inc.

lumencor.com
14940 NW Greenbrier Parkway
Beaverton, OR 97006
Osman Rodriguez - 971-910-0012;
osman.rodriguez@lumencor.com
Adrian Woodland
adrian.woodland@lumencor.com

Marine Reef International

marinereef.com/
1048 Irvine Avenue, Suite 634
Newport Beach, CA 92660
Phone: 949-723-0283
Linda Dailey
903-851-5187; lindasdailey@gmail.com

M.E. Taylor Engineering, Inc.

semsupplies.com
SEMico Division
15817 Crabbs Branch Way
Rockville, MD 20855
Gene Taylor
301-975-9798; sales@semico.org

Molecular Devices, LLC.

moleculardevices.com/
3860 North First Street
San Jose, CA 95134
Phone: 800-635-5577
Robert Moody
469-662-8381; robert.moody@moldev.com

Nanoscience Instruments

nanoscience.com
10008 S 51st St, Phoenix, AZ 85044
Dominic Dominguez
480-758-5424; ddominguez@nanoscience.com

NCI Micro**a Thomas Scientific, LLC company**

ncimicro.com
7125 Northland Terrace N, Suite 100
Brooklyn Park, MN 55428
Phone: 888-559-3312
Mike Hehr
314-374-9361; mike.hehr@thomassci.com
Michael May
405-788-0775; michael.may@thomassci.com

Nikon Instruments Inc.

nikoninstruments.com
1300 Walt Whitman Road
Melville, NY 11747-3064
Phone: 972-693-7779
Jonathan Ekman
407-595-6542; jonathan.ekman@nikon.com
Kara Harmatys
713-301-9932; kara.harmatys@nikon.com
Anil Shukla
407-595-6542; anil.shukla@nikon.com
Renata Tully
469-381-4669; renata.tully@nikon.com

ONI Inc.

oni.bio
11045 Roselle Street, Suite 120
San Diego, CA, 92121
Emanuel Lissek
512-998-9840; emanuel@oni.bio
Regan Moore
512-998-9840; rmoore@oni.bio

Ovation Data

www.ovationdata.com
14199 Westfair East. Dr.,
Houston, TX, 77041-1105, USA
Gregory G. Servos
281-732-4857; gservos@ovationdata.com

Oxford Instruments America, Inc.

oxford-instruments.com
300 Baker Avenue, Suite 150
Concord, MA 01742
Phone: 978-369-9933 x 201
Michael Hjelmstad
987-402-5983; michael.hjelmstad@oxinst.com
Sonika Robertson
987-402-5983; sonika.robertson@oxinst.com



Protochips

protochips.com
3800 Gateway Centre Blvd., Suite 306
Morrisville, NC 27560
Phone: 919-377-0898
Mike Coy
612-751-4391; mike.coy@protochips.com
Gabriela Mendoza - 512-230-6762;
Gabriela.Mendoza@protochips.com
Dylan Wood - 612-751-4391;
Dylan.Wood@protochips.com



RAITH America

raith.com/
300 Jordan Road, Troy, NY 12180
Phone: 518-874-3000
Kevin Burcham - 701-238-1267;
kevin.burcham@raithamerica.com
Joseph Klingfus - 701-238-1267;
Joseph.klingfus@raithamerica.com



Rigaku

rigaku.com
9009 New Trails Dr.
The Woodlands, TX 77381
Phone: 281-362-2300 ext. 122
Angela Criswell
281-362-2300; angela.criswell@rigaku.com
Michelle Goodwin
281-362-2300; Michelle.Goodwin@rigaku.com
Michael Holcomb
281-362-2300; Michael.Holcomb@rigaku.com
Ted Huang
281-362-2300; ted.huang@rigaku.com
Meredith Shi
346-300-2398; meredith.shi@rigaku.com
Aya Takase
281-362-2300; Aya.Takase@rigaku.com
Viral Vaghela
281-362-2300; viral.vaghela@rigaku.com



Scientifica

scientific.us
9 Trenton Lakewood Rd, Clarksburg, NJ 08510
Phone: 470-596-7853
Max Oginsky
max.oginsky@scientific.us
Stephanie Kelly
stephanie.kelly@scientific.us



Microscopy Products for Science and Industry

Ted Pella, Inc.

tedpella.com
PO Box 462477, Redding, CA 96049-2477
Phone: 530-243-2200 or 800-237-3526
James Long
530-227-8329; James_Long@tedpella.com
David Rollings
530-243-2200; sales@tedpella.com
Kathy Stangenberg
530-243-2200; sales@tedpella.com



TESCAN USA, Inc

tescan-usa.com
765 Commonwealth Drive, Suite 101
Warrendale, PA 15086
Phone: 512-417-8990
Mike Craig
724-772-7433; mike.craig@tescan-usa.com
Arnold Hope
724-772-7433; hope.arnold@tescan.com



TEXAS A&M Medicine

Texas A&M University,
School of Medicine
Integrated Microscopy Imaging Laboratory
medicine.tamu.edu/imil/index.html
8447 Riverside Pkwy
Bryan, TX 77807
Malea Murphy
979-436-9037; maleamurphy@tamu.edu
Andrea Trache
281-787-6993; trache@tamu.edu



Texas State University Shared Research Operations

sro.txstate.edu/
601 University Drive
San Marcos, TX 78666
Phone: 512-245-6635
Casey Smith
512-213-7909; cs53360@txstate.edu



Thermo Fisher Scientific / FEI

thermofisher.com
fei.com
Lee Casalena
732-236-5061; lee.casalena@thermofisher.com
Jamie Chermak
971-724-5929;
jamie.chermak@thermofisher.com
K.D. Derr
619-944-7633; kd.derr@thermofisher.com
James Lallo
732-236-5061; james.lallo@thermofisher.com
Bill Sgammato
508-479-6623; bill.sgammato@thermofisher.com
Dan Snyder
346-423-8193; dan.snyder@thermofisher.com
Ciceron Yanez
281-739-7370; ciceron.yanez@thermofisher.com



Tomocube USA

tomocube.com
8880 Rio San Diego Drive, Suite #800
San Diego, CA, 92108
Brian Templin
713-557-8915; templin.b@tomocube.com



Tousimis

tousimis.com
2211 Lewis Avenue
Rockville, MD 20851
Phone: 301-881-2450
Fax: 301-881-5374
Yianni Tousimis
443-254-5423; ytousimis@tousimis.com



The University of Houston College of Optometry

opt.uh.edu/
4401 Martin Luther King Blvd
Houston, TX 77004
Inez Hutchinson
713-743-7593; iajackso@central.uh.edu



The University of Texas at Austin Texas Materials Institute

tmi.utexas.edu
204 E. Dean Keeton Str., Mailstop C2201
Austin, TX 78712
Xun Zhan
216-577-1650; Xun.Zhan@austin.utexas.edu



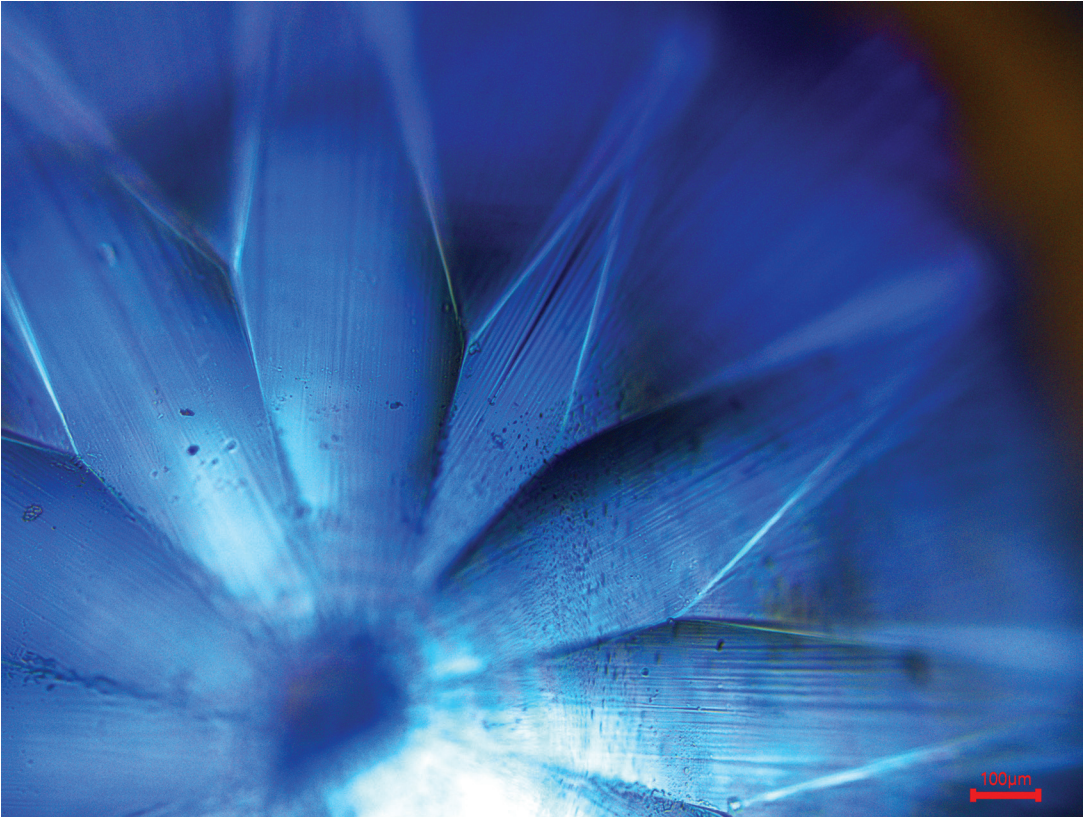
VDURA

vdura.com
2680 North First Street, Suite 150
San Jose, CA 95134
Beth Turman
512-695-8490; bturman@vdura.com



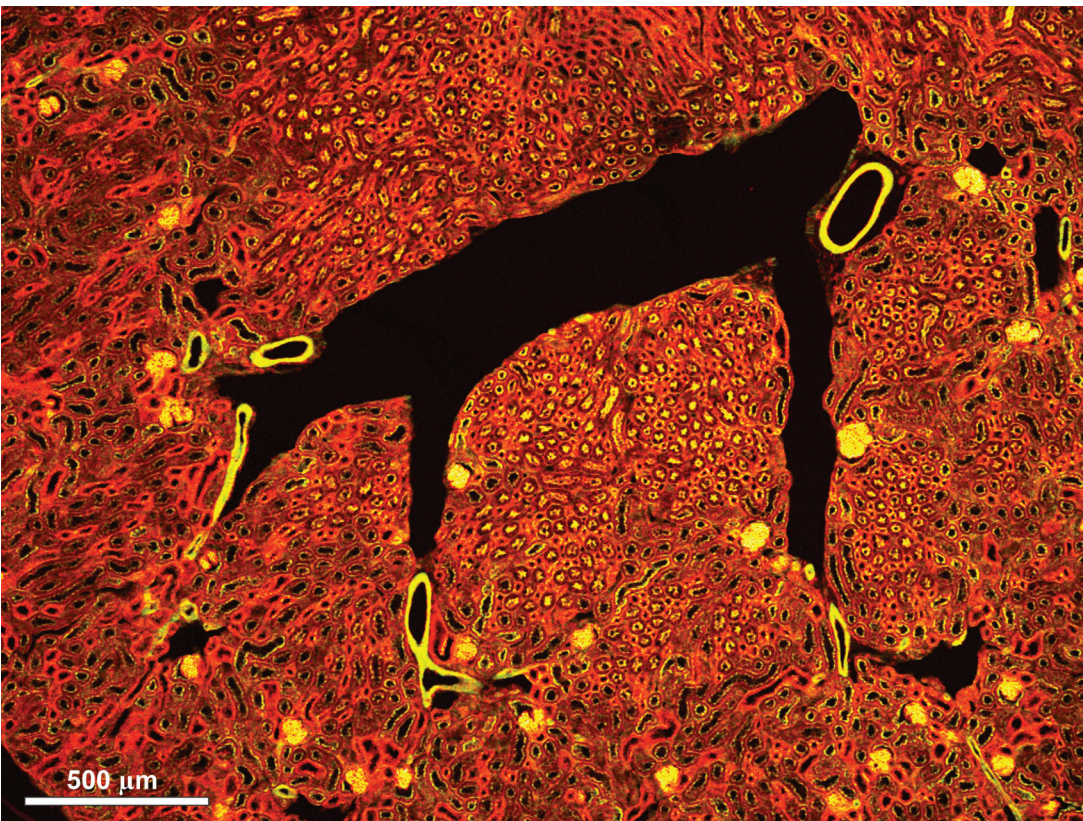
ZEISS MICROSCOPY

zeiss.com/nts
One corporation Way
Peabody, MA 01960
Phone: 978-826-1500
Fax: 978-532-5696 Fax
Laura Grafflin
214-924-7249; laura.grafflin@zeiss.com
Philipp Bastians
914-7471800; philipp.bastians@zeiss.com
John Donlon
800-233-2343; john.donlon@zeiss.com
Steven Hernandez
480-217-9133; steven.hernandez@zeiss.com



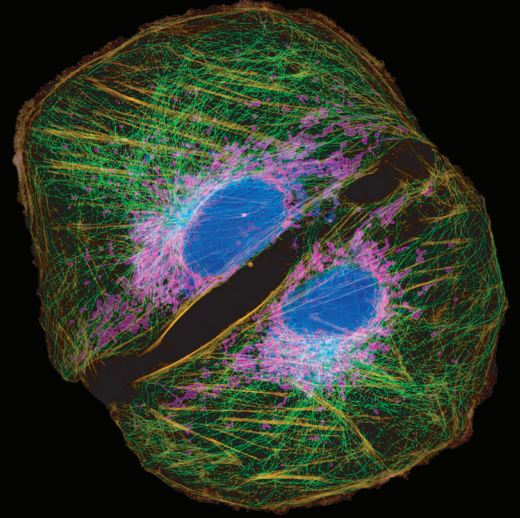
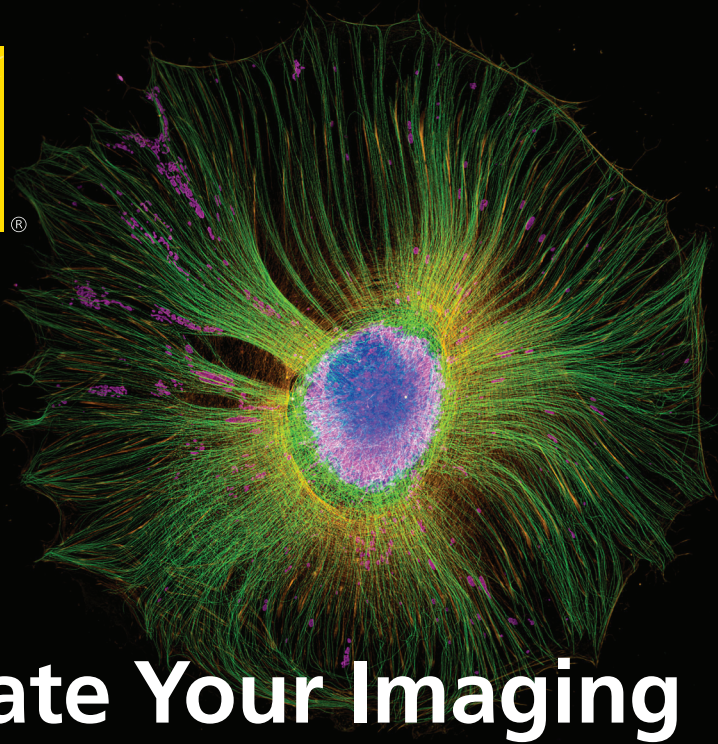
Tanzanite

Image of a tanzanite gem taken with an optical microscope at 5x magnification in bright field mode. The micrograph was obtained by Leona Hazlewood, Instrument Technician at Core Research Operations, Texas State University, San Marcos.



Stained Mouse Kidney

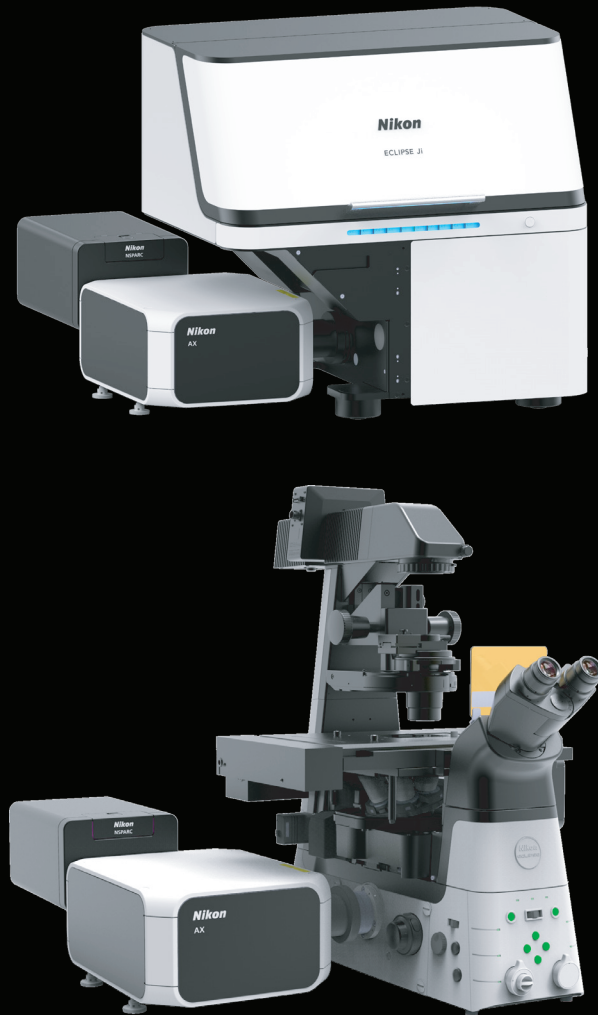
Image of a mouse kidney taken with an Olympus FV3000 Laser Scanning Confocal Microscope at 5x magnification. The micrograph was obtained by Nicki Fairbairn, Scientific Instrument Technician at Shared Research Operations, Texas State University, San Marcos.



Elevate Your Imaging

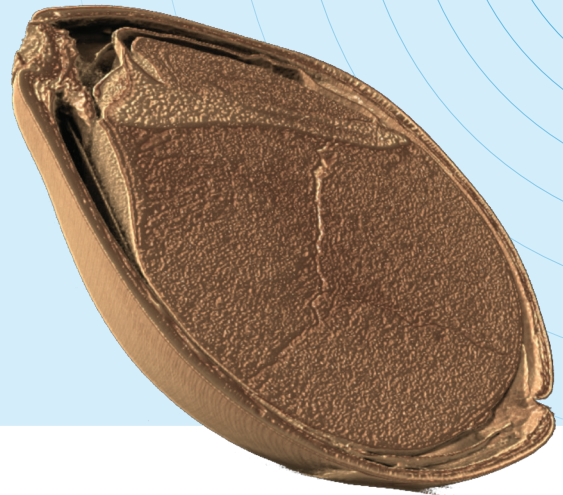
Unlock new research possibilities with Nikon's AX R with NSPARC confocal microscope systems. Single-photon sensitivity and advanced array detection push the boundaries of resolution beyond the theoretical limits. Choose from a range of versatile system configurations to meet your research needs.

To schedule a free microscopy consultation with your Nikon Texas-based microscopy team, contact Amy Leonards at amy.leonards@nikon.com



See What You're Missing

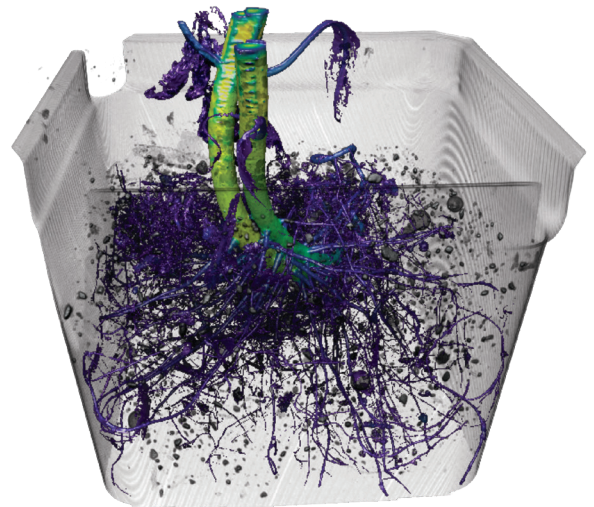
3D X-ray Imaging with
No Sample Prep



X-ray CT requires minimum to no sample prep

Do your current imaging methods require extensive sample preparation that could alter the native state of your biological and organic samples?

X-ray CT can help you see inside your sample, fully intact, in its natural form—without drying, slicing, or coating.



No Sample Prep:

Scan as-is, even wet samples

Non-Destructive:

Preserve sample integrity

3D Insights:

Go beyond the surface and get a 3D volume image

New to CT? We make it easy

Talk to our experts, book a demo, or test your sample.



imaging@rigaku.com
rigaku.com

